

Sensory cortical control of movement

Spyridon K. Karadimas^{1,2,7*}, Kajana Satkunendrarajah^{1,2,3,7*}, Alex M. Laliberte^{2,6}, Dene Ringuette^{2,4}, Iliya Weisspapir², Lijun Li², Simon Gosgnach⁵ and Michael G. Fehlings^{1,2*}

Walking in our complex environment requires continual higher order integrated spatiotemporal information. This information is processed in the somatosensory cortex, and it has long been presumed that it influences movement via descending tracts originating from the motor cortex. Here we show that neuronal activity in the primary somatosensory cortex tightly correlates with the onset and speed of locomotion in freely moving mice. Using optogenetics and pharmacogenetics in combination with in vivo and in vitro electrophysiology, we provide evidence for a direct corticospinal pathway from the primary somatosensory cortex that synapses with cervical excitatory neurons and modulates the lumbar locomotor network independently of the motor cortex and other supraspinal locomotor centers. Stimulation of this pathway enhances speed of locomotion, while inhibition decreases locomotor speed and ultimately terminates stepping. Our findings reveal a novel pathway for neural control of movement whereby the somatosensory cortex directly influences motor behavior, possibly in response to environmental cues.

In the reductionist view, the act of walking, or locomotion, can be considered a simple rhythmic behavior generated by paired oscillators¹. The basic rhythm and pattern associated with walking is generated by a spinal neural network known as the locomotor central pattern generator (CPG)^{2,3}. While the component neurons of the CPG are distributed across numerous spinal cord segments, the interneurons with the greatest rhythmogenic potential are located in the ventromedial aspect (laminae VII, VIII, X) of the lower thoracic and upper lumbar spinal cord⁴ in most mammals studied. To execute purposeful locomotion, activity in the locomotor CPG must first be initiated based on desire/need, and then modulated based on cues from the environment. The cortical and bulbar sites that initiate activity in the locomotor CPG have been well described^{5–12}. These descending inputs play a critical role in initiating and maintaining or halting locomotion^{12,13}. However, walking in the complex environment is directed and executed by the continual detection and integration of multimodal cues¹⁴. It is not known how the higher centers responsible for feedforward and feedback modulation directly control the spinal locomotor circuit in response to higher order somatosensory cues.

It has previously been demonstrated in non-human primates¹⁵, cats¹⁴ and rodents^{16,17} that locomotor-related activity can be encoded from neurons in the primary somatosensory cortex (SI). Interestingly, in some cases, this activity precedes the generation of limb movements¹⁸ and it has been interpreted as anticipatory or predictive. However, it is possible that SI neurons not only encode spatiotemporal information, but that they can also generate a motor response. Indeed, others¹⁹ have demonstrated that the barrel somatosensory cortex forms a parallel motor pathway independent of the motor cortex to direct the whisker system. More recently, optogenetic stimulation of the whisker SI has been shown to evoke short latency retraction of contralateral whiskers²⁰. However, it is unclear whether the role of the sensory cortex in motor control is a general feature, or if it is specific to that of the mouse whisker system. Interestingly, early motor mapping experiments in monkeys²¹ and humans²² have described movements evoked in response

to stimulation of both the SI and the motor cortex. Additionally, in the monkey, retrograde trans-synaptic tracing from finger muscles labeled neurons in the SI. As such, motor control by the sensory cortex may represent a more general phenomenon. Support for the former hypothesis also stems from previous findings demonstrating motor function deficits after lesioning of the sensory cortex^{23,24}. Therefore, it is plausible that the SI participates in controlling locomotion. However, so far there are no studies that have examined whether the SI has a direct and independent motor control of locomotor function.

To examine whether the SI has a direct motor control role on locomotion, we first recorded neuronal activity from the pyramidal neurons of the SI in freely moving mice. We observed a high degree of correlation between the SI neural activity and the speed of movement. Notably, this activity always commenced prior to movement onset, supporting our notion that SI may play a role in initiating and directing movement. Anatomical and electrophysiological probing demonstrated an efferent connectivity between the SI pyramidal neurons and the rhythmogenic regions of the lumbar spinal cord via excitatory interneurons located in the cervical spinal cord. Furthermore, stimulation of these SI neurons increased locomotor speed, while silencing had the opposite effect and impaired the animal's ability to maintain locomotion. Together, our data indicate the existence of a novel neural pathway that enables the somatosensory cortex to directly control movement. We speculate that this pathway, based on integrated information about the environment and the position of the animal within the environment, modulates locomotor activity by directly interfacing with the spinal locomotor network.

Results

SI neuronal activity is highly correlated with the onset and velocity of movement. Initially, we set out to examine whether neurons of the SI participate in the control of locomotion. To this end, we implanted bipolar electrodes in the SI (Fig. 1a) and recorded local field potentials in freely behaving animals while concurrently

¹Division of Neurosurgery, Department of Surgery, University of Toronto, Toronto, Ontario, Canada. ²Krembil Research Institute, University Health Network, Toronto, Ontario, Canada. ³Department of Neurosurgery, Medical College of Wisconsin, Clement J. Zablocki VA Medical Center, Milwaukee, WI, USA.

⁴The Institute of Biomaterials and Biomedical Engineering, University of Toronto, Toronto, Ontario, Canada. ⁵Department of Physiology, University of Alberta, Edmonton, Alberta, Canada. ⁶Present address: Department of Biology, University of Ottawa, Ottawa, Ontario, Canada. ⁷These authors contributed equally: Spyridon K. Karadimas, Kajana Satkunendrarajah. *e-mail: Spyros.Karadimas@mail.utoronto.ca; KajanaS@mcw.edu; Michael.Fehlings@uhn.ca

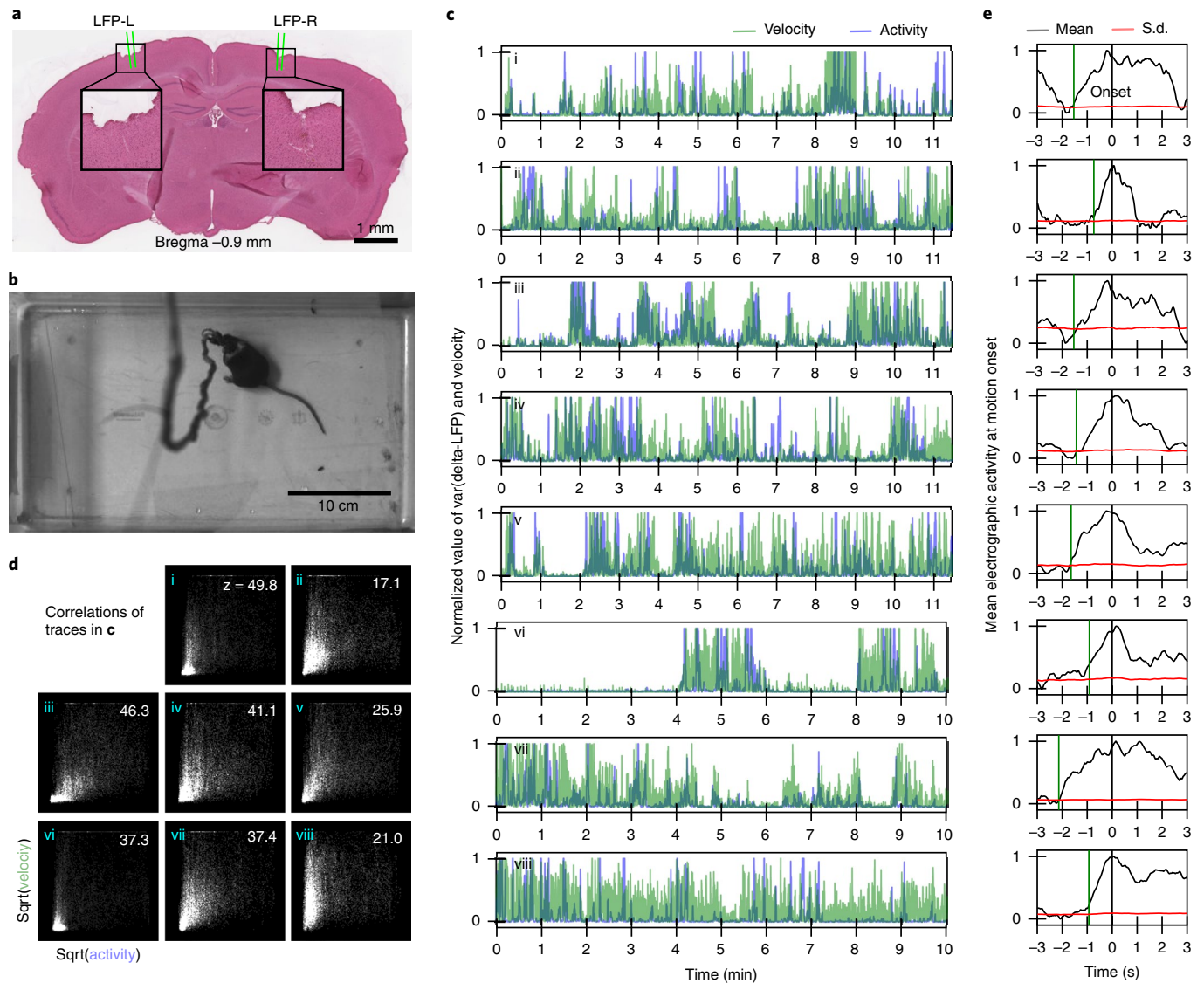


Fig. 1 | Electrophysiological recording of somatosensory activity in freely behaving mice. **a**, Location of implanted penetrating electrodes for recording of the local field potential (LFP). The central target is the SI. **b**, Image taken from concurrent video recording of animal movement and SI activity (see Supplementary Video, which shows the position tracking accuracy). **c**, Velocity of animal locomotion (green trace) and variance of differential somatosensory activity (blue trace), explicitly $\text{var}(\text{LFP}_R - \text{LFP}_L)(t | \Delta t = 1\text{s})$. The difference between contralateral recordings was chosen to isolate asymmetric limb movement during locomotion. **d**, Correlation of animal velocity and somatosensory activity from **c**. The left-to-right orientation in **d** corresponds to the top-to-bottom orientation in **c**; roman numerals in both panels indicate individual mice. The axes were rescaled by the square root (that is, $\text{sqrt}(v(t))$ versus $\text{std}(\text{LFP}_R - \text{LFP}_L)(t | \Delta t = 1\text{s})$). The statistical significance of correlations is indicated by the inset z score (Pearson correlation, $P < 0.001$, $z_{\text{critical}} = 3.2$). Note that the calculated animal positions were digitally low-passed at 5.0 Hz (from the 30 f.p.s. recording) and LFP signals were digitally bandpassed between 0.1 and 50.0 Hz. Sqrt, square root. **e**, Mean electrographic activity at motion onset defined as 10% of maximum locomotion speed from **c**. The detection of activity preceding onset is indicated by vertical lines. ($n = 8$ adult mice for this experiment.).

performing behavioral imaging to track the motion of the mice precisely in an open field setting (Fig. 1b). Quantitative analysis revealed a high degree of correlation between the velocity of locomotion and bilaterally asymmetric changes in local cortical activity (Fig. 1c,d). To examine the temporal specificity of this correlation, frame shifts were applied to the local field potential (LFP) data to disrupt temporal relationships between locomotor velocity and SI activity. Following a forward shift (median = 75 ms, Q1–Q3 = 50–115 ms) and backward shift (median = 195 ms, Q1–Q3 = 125–310 ms) in the LFP, the correlation was reduced below the level of statistical significance (Extended Data Fig. 1), suggesting that the correlation between SI LFPs and locomotor activity is related to their temporal coincidence.

Further analysis indicates that, in all eight animals, SI activity commenced before the onset of, and peaked during, movement (Fig. 1e). The median latency of SI activity to the onset was 1.5 s (Q1–Q3, 0.9–1.6 s) based on the minimum activity weighted temporal skew (Fig. 1e). Thus, we identified that the activity of layer 5 neurons of the SI precedes the onset of movement and is tightly correlated with the speed of locomotion in freely behaving mice, suggesting that SI contributes towards movement initiation and speed programming of locomotion.

Activating pyramidal neurons of the somatosensory cortex triggers neuronal activity in the lumbar spinal cord in vivo. To further understand how SI neuronal activity (Fig. 1) controls

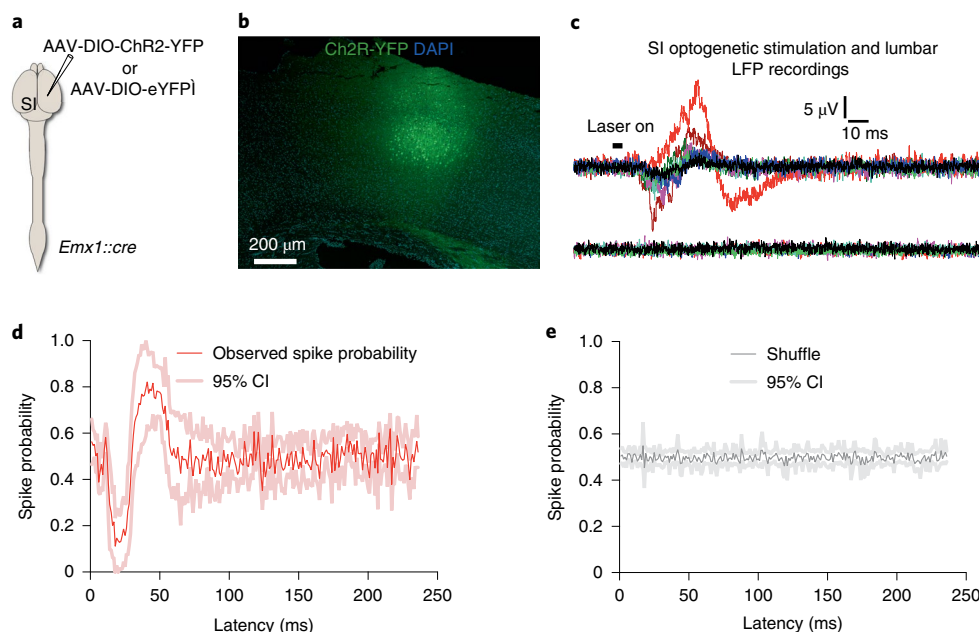


Fig. 2 | Photostimulation of SI pyramidal neurons induces activity in the lumbar cord. **a**, Schematic depicting the strategy used to express ChR2-YFP in the SI pyramidal neurons. **b**, SI pyramidal neurons expressing ChR2-YFP at the AAV-DIO-ChR2-YFP injection site. **c**, In vivo light-evoked lumbar LFP recorded from the lumbar cord area. The traces from individual mice show the lumbar cord field potentials in SI ChR2⁺ (top) or control (bottom) mice before, during and after light stimulation. **d**, Distribution of probability of observing an above-average LFP signal relative to the latency from SI light stimulation. **e**, Probability distribution based on shuffled (1,000 times) trial data (two-sample Kolmogorov-Smirnov test, $n = 8$ mice).

locomotion, we injected an adeno-associated virus (AAV) encoding a *cre*-dependent channelrhodopsin 2 (ChR2)-eYFP (enhanced yellow fluorescent protein) fusion protein (AAV-eYFP-DIO-hChR2-eYFP) into the SI area of *Emx1::cre* mice (Fig. 2a). The targeting specificity to SI layer 5 pyramidal neurons was confirmed post hoc by eYFP fluorescence (Fig. 2b). The SI region of control animals was injected with AAV-eYFP-DIO-eYFP. Two weeks after the injection, a recording electrode was placed into the ventromedial aspect of the rostral lumbar spinal cord containing the rhythmogenic core of the locomotor CPG ('lumbar cord' hereafter) in order to detect field potentials in this region.

Blue light stimulation of the ChR2-expressing SI pyramidal neurons triggered field potentials in the lumbar cord with an average latency of 21.30 ± 0.76 ms (Fig. 2c,d). In contrast, light stimulation did not result in any detectable activity in control mice that received AAV injections lacking the *ChR2* gene (Fig. 2c). To control for the possibility that these responses were the result of spontaneous neuronal activity, a shuffle distribution was generated based on the recordings of the ChR2 mice, effectively removing all temporal information while preserving the activity characteristics of the recordings (Fig. 2d,e). This shuffle distribution was then compared to the average probability distribution of a spike in activity across the recording timescale. We found a statistically significant difference between the two distributions (two-sample Kolmogorov-Smirnov test, $P < 0.001$), suggesting that the activity observed in the lumbar LFP recordings is not random, but is the result of optogenetic stimulation of the SI pyramidal neurons. Given the location of these recordings in the area of the locomotor CPG, these data support an efferent electrical connectivity between the SI and the lumbar spinal locomotor network.

Lack of monosynaptic connectivity between SI and lumbar spinal cord. Next, we used an anatomical approach to investigate whether the SI is directly connected to rhythmogenic neurons in the lumbar spinal cord. The retrograde virus canine adenovirus type-2 (CAV2)-*cre*, containing *LoxP-stop-LoxP* cassettes ahead of

tdTomato, was unilaterally injected into the lumbar segments of Ai9 adult mice (Fig. 3a). This resulted in the expression of the reporter protein tdTomato in all neurons that directly synapse with infected neurons in the lumbar cord. Inspection of the SI in these mice two weeks following injection revealed a lack of labeled neurons in the SI, indicating no direct anatomical connectivity between these regions (Fig. 3b), while the locus coeruleus²⁵ and reticular formation¹², two sites known to play a key role in initiating locomotor activity, contained tdTomato-expressing cells (Fig. 3c). This finding, together with the polysynaptic latency of the lumbar LFPs initiated by SI stimulation, suggests that the SI modulates the lumbar cord via relay neurons.

Stimulation of SI pyramidal neurons increases the frequency of locomotor-like activity. Locomotion in vertebrates is characterized by rhythmic alternation of ipsilateral antagonist, and contralateral agonist, motoneuron pools. This basic rhythmic activity can be observed in the isolated spinal cord in vitro by adding excitatory neurotransmitter agonists to the perfusate. To confirm that the somatosensory cortex is able to modulate locomotion, we developed a new preparation that included the left cerebral hemisphere (with the motor cortex removed), the entire brainstem, and the spinal cord of *Emx1::cre*;Ai27D mouse pups in a three-chamber split bath (Fig. 4a). Using this new preparation, we monitored the L2 (flexor) and L5 (extensor) ventral roots of P0–3 *Emx1::cre*;Ai27D offspring. The expression of ChR2 in cortical pyramidal cells allowed for the selective activation of SI pyramidal cells through the placement of the optical probe in the SI area (Fig. 4b).

The compartment containing the lumbar spinal cord was bathed with minimal concentrations of neuro-active substances NMDA ($5\text{--}7\ \mu\text{M}$) and serotonin (5-HT) ($8\text{--}10\ \mu\text{M}$) that were sufficient to induce slow to intermediate frequency locomotor-like activity (up to 0.5 Hz). To preclude the possibility that SI pyramidal neurons could be acting on the locomotor CPG through other supraspinal centres, kynurenic acid (KA; known to block NMDA and AMPA/kainate receptors) was added in the compartment containing the

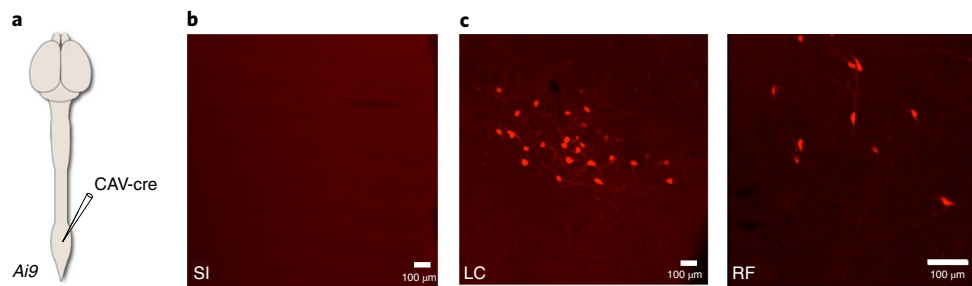


Fig. 3 | Somatosensory cortical connectivity and lumbar spinal cord. **a**, Schematic depicting the strategy used to map connectivity between SI and lumbar cord. **b**, There was a lack of direct SI projections to the lumbar cord, indicated by the absence of any tdTomato⁺ cells in the SI area ($n=3$ mice). **c**, Confocal images of 30- μm -thick transverse sections of the same animal contained tdTomato⁺ cells at the locus coeruleus (LC) and reticular formation (RF), demonstrating direct projection from these regions to the ventromedial area of the upper lumbar spinal cord ($n=3$ mice).

hemibrain and the brainstem (A in Fig. 4a) to block all glutamatergic transmission and neural processing within the cortical and subcortical regions. Optical stimulation of the SI induced an immediate and significant increase in the frequency of locomotor activity (Fig. 4c), demonstrating that the SI acts on the locomotor CPG through a descending corticospinal pathway independently of the motor cortex, brainstem and other supraspinal locomotor centers. Application of the same protocol on Ch2R-negative mice did not alter the locomotor frequency (Extended Data Fig. 2a,b). This evidence, along with the data presented in Fig. 2, indicates that SI activation directly modulates the locomotor CPG without orthodromic or antidromic involvement of the motor cortex or other supraspinal locomotor centers.

SI modulates locomotion via cervical excitatory connections.

Given the lack of direct connectivity between the SI and the rhythmic region of the lumbar cord (Fig. 3b), our next aim was to trace the neural pathway by which the somatosensory cortex modulates activity in the locomotor CPG. Previous work has shown that the cervical spinal cord of mammals receives input from the somatosensory cortex^{26,27} and that neurochemical stimulation of the caudal cervical spinal cord can activate the locomotor CPG²⁸. Here, anterograde tracing from the SI pyramidal neurons using AAVDJ-syn1-DIO-eGFP injected into *Emx1::cre* mice revealed dense innervation in the intermediate gray matter of C4–C7 (Extended Data Fig. 3). Corticospinal axons from the SI project to the dorsomedial laminae III–VII, with highest densities observed in laminae IV and V. The previous findings, along with our current anatomical data, made this region a particularly compelling candidate region for the relay site between the SI and locomotor CPG.

To investigate this, we used the *in vitro* experimental approach described in Fig. 4a. However, this time we recorded locomotor-like activity in response to light stimulation of SI before and after adding KA to the compartment containing the cervical spinal cord (B) to block excitatory transmission within the cervical spinal cord. Following addition of KA in the cervical compartment, photostimulation of the SI had no effect on locomotor frequency (Fig. 4b,c). However, upon washout of KA, photostimulation of SI was once again able to increase the frequency of locomotor-like activity (Extended Data Fig. 4). Together, these data indicate that the output pathway from the SI to locomotor CPG acts via excitatory connections in the cervical enlargement.

SI locomotor pathway plays a critical role in driving locomotion.

To understand how SI neuronal activity translates to the modulation of locomotion *in vivo*, we employed a pharmacogenetic approach to transiently activate or silence the sensory cortical pyramidal neurons projecting to the ventromedial region of the cervical enlargement. A mixture of AAV-DIO-*hM3Dq-mCherry* and

AAV-FLEX^{loxP}-*PSAM^{L141F}-GlyR-IRES-eGFP* was stereotaxically injected bilaterally into the SI two weeks after bilateral *CAV2-cre* injection into the ventromedial region of C4–C5 (Fig. 5a). This injection strategy resulted in the selective expression of *hM3Dq-mCherry*^{29,30} and *PSAM^{L141F}-GlyR/eGFP* (ref. ³¹) in SI pyramidal cells with direct projections to the ventromedial C4–C5 region, allowing their reversible activation or silencing via administration of clozapine N-oxide (CNO) or pharmacologically selective effector molecule (PSEM) 308 (PSEM³⁰⁸), respectively.

Stimulation of this pathway via CNO administration led to a marked increase in the overall speed of locomotion and the distance traveled in an open field setting compared to control saline administration (Fig. 5c). In contrast, inactivation of the pathway via PSEM³⁰⁸ administration diminished the locomotor speed and consequently the distance traveled (Fig. 5b,c). Given the apparent importance of this pathway in governing locomotor speed, spatiotemporal gait parameters were examined during voluntary and uninterrupted passage on a glass walkway. Following SI stimulation, there was an increase in speed and decrease in step cycle duration (Fig. 5d,e), independent of the animal's stride length (Extended Data Fig. 5). As expected, silencing of the SI pathway had the opposite effects on speed and step cycle duration (Fig. 5d,e). Further examination of the effect of SI stimulation using kinematic analysis of hindlimb movements revealed a dramatic increase in acceleration (Fig. 5f,g), potentially contributing to the average increase in locomotor velocity.

In addition to decreasing locomotor speed, silencing of the SI pathway also caused animals to stop more frequently during periods of locomotion. Further analysis of the frequency and duration of spontaneous locomotor bouts from the open field data demonstrated that inhibition of the SI locomotor pathway resulted in a disproportionate decrease (~50%) in the number of locomotor bouts greater than 1 s in duration (Fig. 6a,b). Hence, these data indicate that inhibition of the SI locomotor pathway impairs the animals' ability to maintain ongoing locomotor activity.

Manipulation of the SI locomotor pathway does not alter coordination and paw function.

Importantly, activation and silencing of this pathway did not disrupt balance or coordination³² during locomotion (Extended Data Fig. 5). Manipulation of the SI efferent pathway also did not appear to alter pain sensation, as evidenced by the absence of changes in pain-related parameters of catwalk gait analysis (Extended Data Fig. 6) or the perception of noxious stimuli as assessed by von Frey filament and tail flick tests (Extended Data Fig. 7), thereby excluding the possibility that the increase in locomotor speed is due to increased nociception. Finally, the inactivation of this pathway did not cause any impairment of distal fore- and hindlimb function as measured by fore paw grip strength and catwalk assessments, respectively²³ (Extended Data Figs. 8 and 3, respectively).

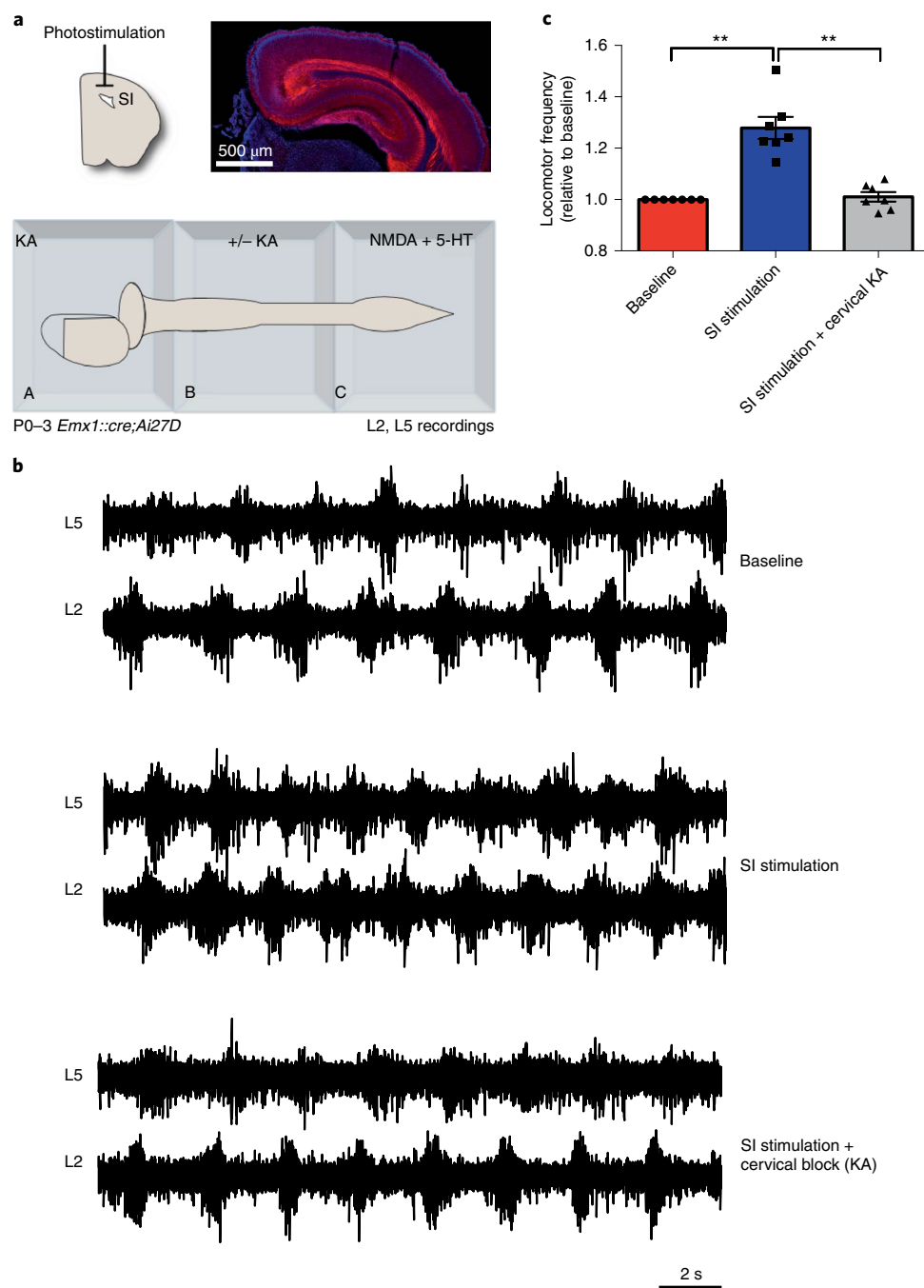


Fig. 4 | The sensory cortex increased the frequency of locomotor-like activity in vitro via cervical excitatory neurotransmission. a, Schematic of the design for electrophysiological experiments in the hemicortex-whole brainstem-spinal cord preparations from P0–P3 postnatal mouse pups. The hemicortical section of the *Emx1::cre;Ai27D* mouse pup demonstrates Ch2R expression in the cortex and shows the position where the optical probe was placed. Note that the optical probe was placed on the cortical surface and a needle was inserted at the end to anatomically confirm the location. **b**, Representative electroneurogram (ENG) recordings of locomotor-like activity from ipsilateral L2 and L5 ventral roots induced with 7 μM NMDA and 10 μM 5-HT. Application of KA to the bath containing the brain and brainstem blocked all glutamatergic transmission. Optogenetic stimulation of the SI neurons increased the frequency of locomotor-like bursting activity (middle). Application of KA to the bath containing the cervical spinal cord blocked SI recruitment of cervical neurons and prevented the increase in the frequency of locomotor-like activity (bottom). **c**, Relative change in frequency of locomotor-like activity before optical stimulation of SI (red), during stimulation (blue) and during stimulation with KA in the cervical bath (gray). ** $P < 0.01$. $n = 7$ mice. Data are presented as mean \pm s.e.m.

SI motor signal is relayed to the locomotor CPG via cervical excitatory interneurons. To refine the characterization of the corticospinal locomotor pathway controlled by SI, we aimed to confirm that the relay neurons located in the cervical cord are excitatory using a multipronged approach consisting of in vivo electrophysiology

and cellular-specific pharmacogenetics. Initially we characterized the spatial distribution of cervical excitatory interneurons (eINs) projecting to the lumbar spinal cord using an intersectional strategy on the double transgenic *Slc17a6* (hereafter referred to as *Vglut2*::*cre;Ai65* mice. These mice allow for the conditional

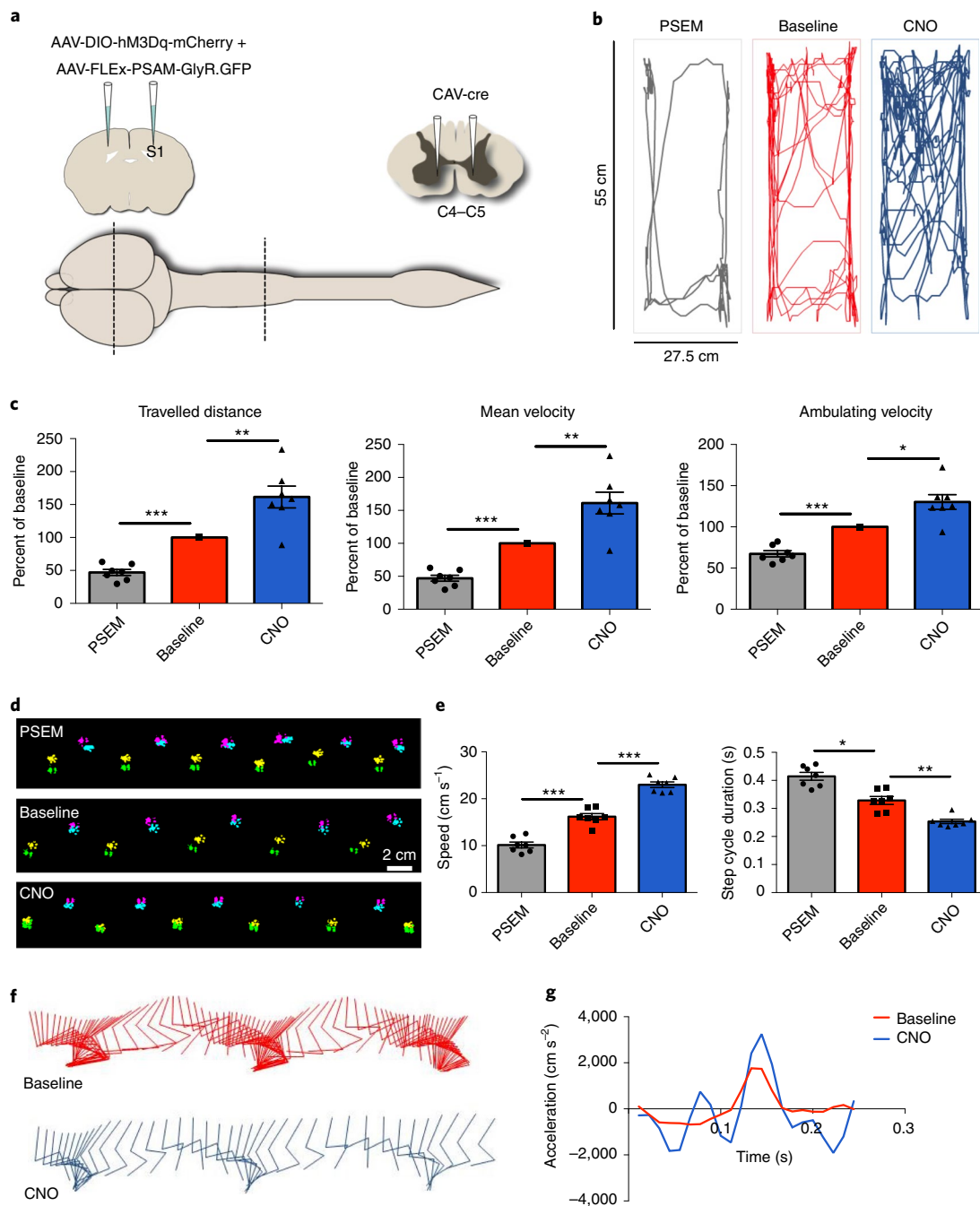


Fig. 5 | Sensory cortex regulates locomotor output. **a**, Schematic demonstrating the approach utilized to express hM3Dq-mCherry or PSAM^{L141FY115F}-GlyR/GFP in the pyramidal SI neurons projecting to the intermediate gray matter of cervical enlargement. **b**, Representative traces of movements for 5 min in an open field at baseline (middle, red) and after CNO (right, blue) or PSEM (left, gray) administration. **c**, Graphs (from all animals) of the total distance travelled, the mean velocity (including stops) and the average velocity of ambulation (excluding stops). **d**, Foot placements of the animals while crossing the walkway (light blue, right front paw; yellow, left front paw; green, left hind paw; purple, right hind paw). **e**, Graphs showing the effects on speed and step cycle duration during spontaneous and uninterrupted passage on a walkway at baseline (red) and after inhibition (PSEM, gray) or stimulation (CNO, blue) of the SI locomotor pathway. **f**, Kinematic representation of the relative positions of the toe, ankle, knee and hip before (left) and after (right) CNO administration. **g**, Corresponding relative acceleration of ankle during this locomotor behavior. Repeated measures one-way ANOVA with Dunnett's multiple comparison; *** $P < 0.001$, ** $P < 0.01$ and * $P < 0.05$. $n = 7$ mice. Group data are presented as mean \pm s.e.m.

expression of tdTomato in only the excitatory cells that express the flippase (*Flp*) recombinase. Injection of the retrograde CAV2-FLEX^{loxP}-*Flp* (ref. ³³) into the lumbar cord of these mice resulted in the expression of the FLP and the subsequent expression of tdTomato in only the lumbar projecting excitatory neurons. Inspection of the cervical spinal cords showed a high density of excitatory

lumbar-projecting cervical neurons to be located in laminae VII and X of the cervical spinal cord, with the majority of them spanning C4–C5 spinal segments (Extended Data Fig. 9). These results along with those described in Extended Data Fig. 3 indicate that the cervical excitatory cells that relay the SI motor signal reside in the intermediate gray matter of C4–C5 segments.

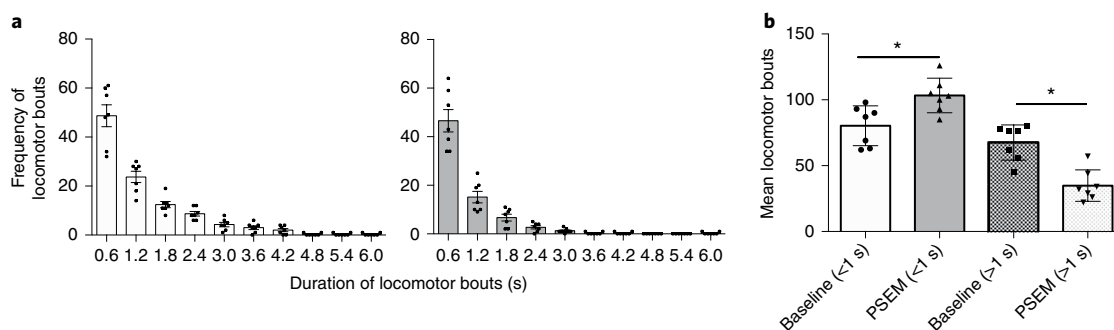


Fig. 6 | The sensory cortical pathway is necessary for maintenance of locomotion. **a**, Histogram demonstrating the average frequency of locomotor bouts of different durations at baseline (white) and after PSEM injection (gray) over 5 min intervals in an open field. **b**, Graph showing the average frequencies of locomotor bouts lasting less than 1 s and longer than 1 s. Mice given PSEM to silence SI locomotor neurons have fewer locomotor bouts longer than 1 s, but also have more short-duration locomotor events when compared to baseline. Wilcoxon matched-pair signed-rank test. In all panels, *** $P < 0.001$, ** $P < 0.01$ and * $P < 0.05$, respectively. $n = 7$ mice. Data are presented as mean \pm s.e.m.

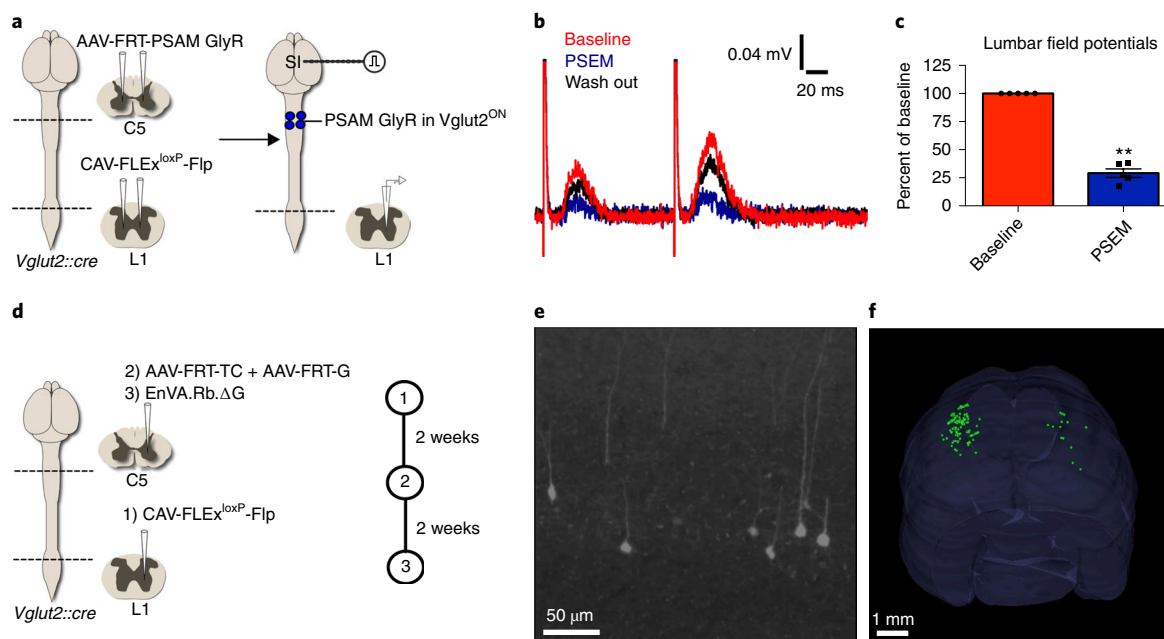


Fig. 7 | Cervical eINs relay the SI motor signal to the lumbar spinal cord. **a**, Schematic depicting the strategy used to express PSAM GlyR in only the lumbar-projecting glutamatergic cells residing in the intermediate gray matter of C4–C5. **b**, Field potential recordings in the ventromedial region of the upper lumbar spinal cord following SI stimulation before (red) and after (blue) PSEM administration (i.p.) and after washout of PSEM (black). **c**, Amplitude of lumbar field potentials before and 40 min after PSEM administration ($n = 4$ mice). Paired Student's t -test; *** $P < 0.001$, ** $P < 0.01$ and * $P < 0.05$. Data are presented as mean \pm s.e.m. **d**, Viral experimental strategy to demonstrate anatomically the SI–cervical eINs–lumbar spinal cord pathway ($n = 3$ mice). **e**, Representative images of the somatosensory regions providing input to excitatory neurons of the ventromedial area of the C4–C5 spinal segments that project to the ventromedial area of the upper lumbar spinal cord. Imaging was performed in three mice with similar results. **f**, Reconstruction of the brain demonstrating that cells in the SI are connected to the rhythmogenic center of the locomotor CPG via glutamatergic cells in the C4–C5 segments.

To confirm whether indeed these cervical eINs comprise the relay between the SI and lumbar spinal cord, CAV2-FLEX^{loxP}-Flp was bilaterally injected within the lumbar cord of *Vglut2::cre* mice (Fig. 7a). Two weeks later the C4–C5 spinal cord was bilaterally injected with AAV-FLEX^{FRT}-PSAM^{L141FY115F}-GlyR (Fig. 7a). This injection paradigm resulted in expression of the PSEM-dependent chimeric receptor/chloride channel in only those excitatory cells in the C4–C5 spinal segments that project axons to the region containing the bulk of the rhythmogenic components of the locomotor CPG⁷. Two weeks following the injections, electrical stimulation of the SI region evoked field potentials in the intermediate gray matter of the lumbar cord (Fig. 7b). Transient inhibition of the

lumbar-projecting eINs in the C4–C5 segments via PSEM³⁰⁸ administration resulted in a substantial decrease in the amplitude of the evoked field potentials recorded in the lumbar cord (Fig. 7b,c). These data indicate that the primary sensory cortex has efferent control of the locomotor related regions of the lumbar spinal cord via eINs in the cervical spinal cord.

Further anatomical support for this pathway came from experiments using cellular specific monosynaptic tracing originating from the lumbar projecting cervical eINs. Specifically, retrograde CAV2-FLEX^{loxP}-Flp was injected unilaterally into the lumbar cord of *Vglut2::cre* mice. This resulted in the expression of Flp recombinase in all the eINs projecting to the lumbar cord. Injection of

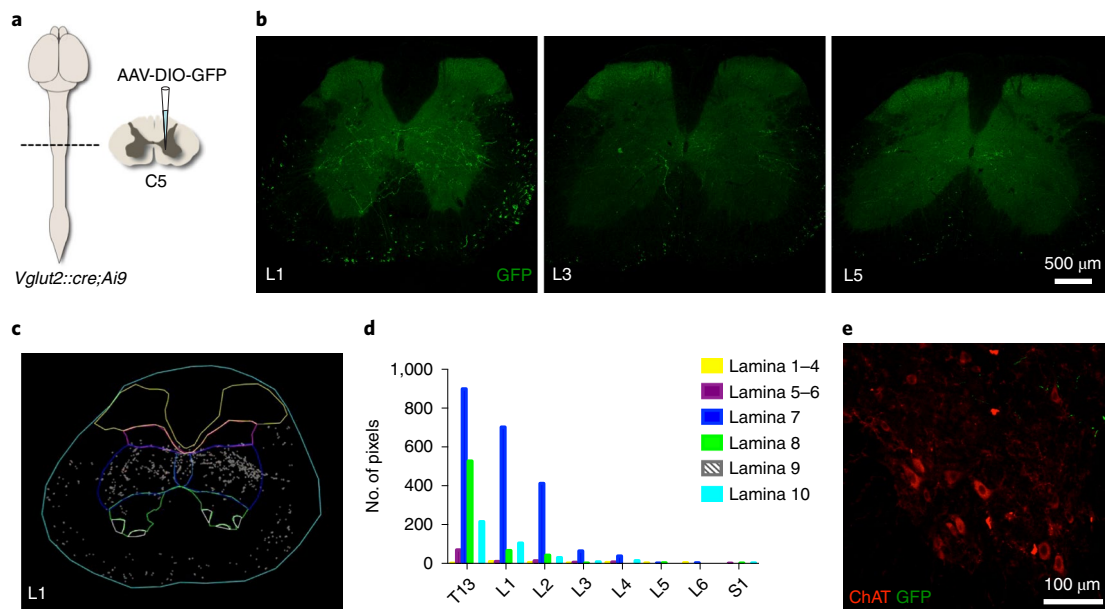


Fig. 8 | Cervical excitatory cells project predominantly to lamina VII of the upper lumbar spinal cord. a, Unilateral injection of a Cre-dependent AAV-*Syn1-DIO-eGFP* virus in the ventromedial area of C4–5 spinal segments of *Vglut2::cre;tdTomato* mice ($n = 3$ mice). **b**, Transverse lumbar spinal cord sections showing GFP-labeled projections from transfected *Vglut2^{ON}* neurons from ventromedial C4–5. No projections were identified in the dorsal and anterior horns. Imaging performed in three mice with similar results. **c**, Example of a reconstructed transverse spinal cord section with GFP projections using NeuroLucida software. **d**, Quantification in one animal of the number of fluorescent pixels in each lamina and at different spinal levels using NeuroLucida. **e**, Lack of putative contacts of cervical eINs of the ventromedial region with lumbar motoneurons (ChAT⁺). Imaging performed in three mice with similar results.

AAV-FLEX^{FRT}-TC/G³⁴ into the ipsilateral ventromedial region of C4–C5 (Fig. 7d) resulted in the expression of rabies glycoprotein (G) and the TVA (receptor for EnvA) in the lumbar-projecting cervical eINs. Because only the lumbar-projecting cervical eINs expressed G and TVA, subsequent cervical injection of EnvA-coated, G-deleted rabies viruses (RVdG) resulted in trans-synaptic spread to presynaptic neurons of lumbar-projecting cervical eINs. A robust population of pyramidal cells in the SI area connected to the rhythmogenic center of the locomotor CPG via cervical eINs was identified (Fig. 7e,f).

These results suggest that the SI promotes movement by activating rhythm-generating circuits in the lumbar spinal cord via cervical eINs. To further support the existence of this pathway, we performed anterograde labeling of the eINs that reside in laminae IV–VII and X of the C4–C5 spinal levels—an area that receives dense projections from the SI pyramidal neurons (Extended Data Fig. 3). Cervical eINs of the intermediate gray matter had extensive GFP⁺ fiber tracts in the ventromedial area of the upper lumbar spinal cord (T13–L2) where locomotor neurons with highest rhythmogenic potential are located^{3,35–37} (Fig. 8). No innervation was found in the dorsal horn and in the ventral horns. Indeed, motor neurons showed no somatic contacts from the labeled cervical eINs (Fig. 8e).

Discussion

Locomotion is often considered to be a simple behavior, consisting of rhythmic alternation of flexor and extensor motor pools on the left and right sides of the body. However, to navigate the complex environment in which we live, the locomotor neural network in the spinal cord relies heavily on feedback control from sensory fibers²⁶ and feedforward control from higher centers such as the visual cortex²⁷. Classical studies of mammalian movement control define a prominent role for the primary motor cortex³⁸. Activity in SI neurons has been shown previously to have a modulatory role in locomotor activity in primates¹⁵, cats¹⁴ and rodents^{16,17}. These earlier

studies had interpreted this activity to be mainly anticipatory and exerted via the motor cortex. Here, we provide evidence for a parallel pathway from the SI that descends directly to the spinal cord and is able to modulate locomotor output.

Only relatively recently has it been demonstrated that SI modulates motor behaviors such as whisking²⁰. Formerly, the whisker motor cortex (wM1) was thought to exclusively direct whisker motor control³⁹. However, previous research demonstrated that animals with a frontal cortex lesion (including wM1) could still whisk, raising the possibility that other regions may participate in the control of whisking⁴⁰. Similar to the SI activity observed during locomotion, active whisking had been correlated to changes in SI cortical neuronal discharges⁴¹. Subsequent work demonstrated that a direct motor control pathway for the mouse whisker system is driven by SI independently of the motor cortex¹⁹. These studies, together with the finding that SI decodes motor-related signals in mouse V1^{42,43}, suggested that SI cortical activity is not purely related to sensory processing; however, it was not known if these findings could be generalized to other motor systems.

In this study, we use both intact adult and in vitro hemibrain-intact mouse preparations to demonstrate that pyramidal neurons in SI play a critical role in the control of locomotor activity. This emerged from our initial finding that SI pyramidal neurons are active during spontaneous overground locomotion in adult mice, and is in agreement with previous work reporting SI activity during quadrupedal or bipedal locomotion^{14,16,17}. In our experiments, SI activity was highly correlated to the speed of locomotor activity and, importantly, preceded the onset of movement. This suggests that SI activity during stepping is not purely encoding information related to the animal's position in the environment, but may also include specific motor commands based on the integration of related sensory information. Support for the latter conclusion first came from our in vitro behavioral experiments. Using a combination of optogenetics, pharmacology and a mouse neonatal in vitro fictive

locomotor preparation, we found that SI stimulation increases the frequency of locomotor-related activity without altering locomotor pattern. Notably, these *in vitro* experiments took place while the connections in the brain and brainstem were pharmacologically silenced, with the motor cortex surgically removed, and in the absence of any sensory feedback. These data provide strong evidence that SI neurons are able to modulate activity of the locomotor CPG independently of other brain and brainstem regions.

This hypothesis was further supported by our demonstration that neuronal activity can be triggered in the lumbar spinal cord in response to stimulation of the SI pyramidal neurons in the adult mouse. Pharmacogenetic activation of SI pyramidal neurons that project to the cervical spinal cord led to a significant increase in the overall speed of locomotion in freely moving mice. In contrast, inactivation of this pathway not only reduced the speed of locomotion but substantially impaired locomotion, demonstrating the necessity of the SI locomotor pathway in locomotor control. Taken together, these results identify an efferent pathway from SI to the lumbar spinal cord via cervical eINs and demonstrate a role for this pathway in the control of locomotion. As such, we believe that the somatosensory cortex, based on integrated information related to the state of the animal and its surroundings, encodes a motor command signal. However, the precise nature of the sensory processing, and the mechanism by which the motor signal is generated in the sensory cortex, require further examination.

SI pyramidal neurons project to the contralateral intermediate gray matter of the cervical spinal cord, mainly in the C4–C5 area. Interestingly, our data also show this area to contain most of the excitatory cells that project to the lumbar cord. These excitatory cells of the C4–C5 intermediate gray matter area project to the rhythmogenic area of the locomotor CPG without making any detectable synaptic contacts with the lumbar motoneurons. Moreover, in line with previous work⁴⁴, our Vglut2-restricted monosynaptic retrograde tracing demonstrates that SI neurons have efferent connectivity to the lumbar locomotor region via cervical excitatory interneurons. Additional support for the excitatory nature of the cervical INs was provided by pharmacogenetic silencing experiments in adult anesthetized mice, demonstrating that the cervical eINs within C4–C5 are required for the observed efferent connectivity between SI and the lumbar spinal cord. Collectively, these anatomical and electrophysiological results demonstrate functional connectivity between SI pyramidal neurons and rostral lumbar spinal cord neurons via cervical eINs, a pathway that is likely responsible for conveying the SI motor signal to the locomotor CPG.

In summary, we show that part of the activity generated in the somatosensory cortex prior and during movement represents a motor signal. This SI motor signal projects to the spinal cord, bypassing the motor cortex and other locomotor areas. The proposed SI locomotor pathway is distinct from previously identified mechanisms of cortical locomotor control from the motor cortex (gait modifications) and posterior parietal cortex (motor planning)²⁷, and provides a potential mechanism to directly and efficiently modulate movement according to sensorimotor information. These data add to a growing body of evidence suggesting that the somatosensory cortex, which receives and integrates information about our everchanging internal and external environment, plays a significant role in the direct control of movement.

Online content

Any methods, additional references, Nature Research reporting summaries, source data, extended data, supplementary information, acknowledgements, peer review information; details of author contributions and competing interests; and statements of data and code availability are available at <https://doi.org/10.1038/s41593-019-0536-7>.

Received: 29 January 2019; Accepted: 8 October 2019;
Published online: 18 November 2019

References

- Andersson, O., Forsberg, H., Grillner, S. & Wallen, P. Peripheral feedback mechanisms acting on the central pattern generators for locomotion in fish and cat. *Can. J. Physiol. Pharmacol.* **59**, 713–726 (1981).
- Kiehn, O. Locomotor circuits in the mammalian spinal cord. *Annu. Rev. Neurosci.* **29**, 279–306 (2006).
- Kiehn, O. Decoding the organization of spinal circuits that control locomotion. *Nat. Rev. Neurosci.* **17**, 224–238 (2016).
- Kjaerulf, O. & Kiehn, O. Distribution of networks generating and coordinating locomotor activity in the neonatal rat spinal cord *in vitro*: a lesion study. *J. Neurosci.* **16**, 5777–5794 (1996).
- Drew, T. Motor cortical activity during voluntary gait modifications in the cat. I. Cells related to the forelimbs. *J. Neurophysiol.* **70**, 179–199 (1993).
- Garcia-Rill, E. & Skinner, R. D. The mesencephalic locomotor region. I. Activation of a medullary projection site. *Brain Res.* **411**, 1–12 (1987).
- Hagglund, M., Borgius, L., Dougherty, K. J. & Kiehn, O. Activation of groups of excitatory neurons in the mammalian spinal cord or hindbrain evokes locomotion. *Nat. Neurosci.* **13**, 246–252 (2010).
- Jankowska, E., Nilsson, E. & Hammar, I. Processing information related to centrally initiated locomotor and voluntary movements by feline spinocerebellar neurons. *J. Physiol.* **589**, 5709–5725 (2011).
- Matsuyama, K. et al. Locomotor role of the corticoreticular–reticulospinal–spinal interneuronal system. *Prog. Brain Res.* **143**, 239–249 (2004).
- Shefchyk, S. J., Jell, R. M. & Jordan, L. M. Reversible cooling of the brainstem reveals areas required for mesencephalic locomotor region evoked treadmill locomotion. *Exp. Brain Res.* **56**, 257–262 (1984).
- Steeves, J. D. & Jordan, L. M. Localization of a descending pathway in the spinal cord which is necessary for controlled treadmill locomotion. *Neurosci. Lett.* **20**, 283–288 (1980).
- Bouvier, J. et al. Descending command neurons in the brainstem that halt locomotion. *Cell* **163**, 1191–1203 (2015).
- Gordon, I. T. & Whelan, P. J. Brainstem modulation of locomotion in the neonatal mouse spinal cord. *J. Physiol.* **586**, 2487–2497 (2008).
- Favorov, O. V., Nilaweera, W. U., Miasnikov, A. A. & Beloozerova, I. N. Activity of somatosensory-responsive neurons in high subdivisions of SI cortex during locomotion. *J. Neurosci.* **35**, 7763–7776 (2015).
- Fitzsimmons, N. A., Lebedev, M. A., Peikon, I. D. & Nicolelis, M. A. Extracting kinematic parameters for monkey bipedal walking from cortical neuronal ensemble activity. *Front. Integr. Neurosci.* **3**, 3 (2009).
- Chapin, J. K. & Woodward, D. J. Somatic sensory transmission to the cortex during movement: gating of single cell responses to touch. *Exp. Neurol.* **78**, 654–669 (1982).
- Chapin, J. K. & Woodward, D. J. Somatic sensory transmission to the cortex during movement: phasic modulation over the locomotor step cycle. *Exp. Neurol.* **78**, 670–684 (1982).
- London, B. M. & Miller, L. E. Responses of somatosensory area 2 neurons to actively and passively generated limb movements. *J. Neurophysiol.* **109**, 1505–1513 (2013).
- Matyas, F. et al. Motor control by sensory cortex. *Science* **330**, 1240–1243 (2010).
- Auffret, M. et al. Optogenetic stimulation of cortex to map evoked whisker movements in awake head-restrained mice. *Neuroscience* **368**, 199–213 (2018).
- Sessle, B. J. & Wiesendanger, M. Structural and functional definition of the motor cortex in the monkey (*Macaca fascicularis*). *J. Physiol.* **323**, 245–265 (1982).
- Wilder Penfield, E. B. Somatic motor and sensory representation in the cerebral cortex of man as studied by electrical stimulation. *Brain* **60**, 389–443 (1937).
- Błaszczak, J. W. & Dobrzecka, C. Effects of unilateral somatosensory cortex lesion upon locomotion in dogs. *Acta Neurobiol. Exp. (Wars.)* **55**, 133–140 (1995).
- Richardson, A. G. et al. The effects of acute cortical somatosensory deafferentation on grip force control. *Cortex* **74**, 1–8 (2016).
- Clark, F. M. & Proudfit, H. K. The projection of locus coeruleus neurons to the spinal cord in the rat determined by anterograde tracing combined with immunocytochemistry. *Brain Res.* **538**, 231–245 (1991).
- Wise, S. P. & Jones, E. G. Cells of origin and terminal distribution of descending projections of the rat somatic sensory cortex. *J. Comp. Neurol.* **175**, 129–157 (1977).
- Ueno, M. et al. Corticospinal circuits from the sensory and motor cortices differentially regulate skilled movements through distinct spinal interneurons. *Cell Rep.* **23**, 1286–1300 (2018).
- Cowley, K. C. & Schmidt, B. J. Regional distribution of the locomotor pattern-generating network in the neonatal rat spinal cord. *J. Neurophysiol.* **77**, 247–259 (1997).

29. Alexander, G. M. et al. Remote control of neuronal activity in transgenic mice expressing evolved G protein-coupled receptors. *Neuron* **63**, 27–39 (2009).
30. Armbruster, B. N., Li, X., Pausch, M. H., Herlitze, S. & Roth, B. L. Evolving the lock to fit the key to create a family of G protein-coupled receptors potently activated by an inert ligand. *Proc. Natl Acad. Sci. USA* **104**, 5163–5168 (2007).
31. Magnus, C. J. et al. Chemical and genetic engineering of selective ion channel–ligand interactions. *Science* **333**, 1292–1296 (2011).
32. Bellardita, C. & Kiehn, O. Phenotypic characterization of speed-associated gait changes in mice reveals modular organization of locomotor networks. *Curr. Biol.* **25**, 1426–1436 (2015).
33. Keriél, A., Rene, C., Galer, C., Zabner, J. & Kremer, E. J. Canine adenovirus vectors for lung-directed gene transfer: efficacy, immune response and duration of transgene expression using helper-dependent vectors. *J. Virol.* **80**, 1487–1496 (2006).
34. Schwarz, L. A. et al. Viral-genetic tracing of the input–output organization of a central noradrenergic circuit. *Nature* **524**, 88–92 (2015).
35. Goulding, M. Circuits controlling vertebrate locomotion: moving in a new direction. *Nat. Rev. Neurosci.* **10**, 507–518 (2009).
36. Grillner, S. & Jessell, T. M. Measured motion: searching for simplicity in spinal locomotor networks. *Curr. Opin. Neurobiol.* **19**, 572–586 (2009).
37. McLean, D. L. & Dougherty, K. J. Peeling back the layers of locomotor control in the spinal cord. *Curr. Opin. Neurobiol.* **33**, 63–70 (2015).
38. Wise, S. P. The primate premotor cortex: past, present and preparatory. *Annu. Rev. Neurosci.* **8**, 1–19 (1985).
39. Petersen, C. C. Cortical control of whisker movement. *Annu. Rev. Neurosci.* **37**, 183–203 (2014).
40. Semba, K. & Komisaruk, B. R. Neural substrates of two different rhythmical vibrissal movements in the rat. *Neuroscience* **12**, 761–774 (1984).
41. Crochet, S. & Petersen, C. C. Correlating whisker behavior with membrane potential in barrel cortex of awake mice. *Nat. Neurosci.* **9**, 608–610 (2006).
42. Niell, C. M. & Stryker, M. P. Modulation of visual responses by behavioral state in mouse visual cortex. *Neuron* **65**, 472–479 (2010).
43. Keller, G. B., Bonhoeffer, T. & Hubener, M. Sensorimotor mismatch signals in primary visual cortex of the behaving mouse. *Neuron* **74**, 809–815 (2012).
44. Ruder, L., Takeoka, A. & Arber, S. Long-distance descending spinal neurons ensure quadrupedal locomotor stability. *Neuron* **92**, 1063–1078 (2016).

Publisher's note Springer Nature remains neutral with regard to jurisdictional claims in published maps and institutional affiliations.

© The Author(s), under exclusive licence to Springer Nature America, Inc. 2019

Methods

Mouse lines. All experiments were performed in accordance with Canadian Council on Animal Care guidelines and were approved by the University Health Network's animal research committee. C57BL/6J mice (Jackson Labs, #000664), *Vglut2::cre* mice (B6-*Slc17a6*^{tm2(cre)Low1}/J, Jackson Labs, #016963), Ai9 mice (B6.129S-Gt(Rosa)Sor26^{tm9(CAG-tdTomato)Hze}/J, Jackson Labs, #007908), Ai65 mice (B6.129S-Gt(Rosa)Sor26^{tm65.1(CAG-tdTomato)Hze}/J, Jackson Labs, #021875), Ai27D mice (B6.Cg-Gt(Rosa)26Sor^{tm27.1(CAG-COP4^{H134R}/tdTomato)Hze}/J, Jackson Labs, #012567) and *Emx1::cre* mice (B6.129S2-*Emx1*^{tm1(cre)Kri}/J, Jackson Labs, #005628) were purchased from commercial vendors.

Surgical procedures. For all surgical procedures mice were anesthetized using 2% isoflurane at 1 l min⁻¹ (O₂ carrier gas) in an induction chamber with maintenance at 1.0–1.5% isoflurane via a nose cone. Buprenorphine (0.05 mg kg⁻¹) was administered subcutaneously for analgesia. Post-operative buprenorphine was administered.

Surgical implantation of chronic intracranial electrodes. For this experiment we used six-week-old C57BL/6J male mice. Bipolar twisted-metal electrodes (200 μm diameter; MS303/3-B/SPC, Plastics One) were implanted bilaterally through two 1 mm burr holes drilled in the skull (bregma -0.9 mm, lateral 1.9 mm and depth 0.5 mm) in the SIs. A unipolar ground electrode was placed caudal to the recording region external to the meninges. Dental cement (A-M Systems models 525000 and 526000) was used to secure the implanted electrodes, ground electrode (support screw interparietal bone) and additional anchoring (dedicated screw in frontal bone).

Behavioral imaging system for concurrent recording of somatosensory electrographic activity. The cortical LFP was amplified using a DP-304 differential amplifier (Warner Instruments) and digitized using a CED Micro1401-3 unit (Cambridge Electronic Design). Once electrographic recording was initiated, the movements of the freely behaving mice were recorded using a camera (Retiga4000R, Q-Imaging) mounted 0.7–0.8 m above an enclosure of dimensions are 42 × 26 cm. A Nikon Nikkor 24 mm lens (SLR with focal length set at 1.2 m and f/8.0 aperture) was used to keep the mouse in focus. The camera was operated using Micro-manager 1.4 acquisition software with 4 × 4 pixel binning and 10 ms exposure with frames acquired at 26 Hz or 30 Hz (dependent on the frame buffering scheme). Animals were interfaced with the electrographic recording apparatus for no more than 15 min. The intracranial LFP was sampled at 10 kHz with an active high-pass filter (1 Hz) and an active low-pass filter (3 kHz) applied through the amplifier. The camera's frame-capture triggers were recorded at 10 kHz using the same digitizer to correlate movement and electrical activity.

Animal tracking analysis and electrographic data processing. The camera trigger traces were low-pass filtered at 60 Hz with zero-phase delay using forward and backward application of an RC filter. Maximum values of the filtered signal were used to define precise frame-capture time points. The 8 bit images were inverted (that is, $I_{new} = 255 - I_{old}$) and spatially mean filtered with 7 × 7 pixel binning. Images were threshold subtracted (between 230–240 gray levels). Location coordinates were estimated as the new intensity weighted mean. The location coordinates were low-pass filtered at 5 Hz (same zero-phase delay scheme) to remove the influence of electrode cables on location estimation from the videos. Coordinate accuracy was confirmed by observation of a superimposed spot on the videos. Animal velocity was calculated from the difference between sequential planar coordinates extracted in this manner. Velocity values were winsorized at four standard deviations to remove the influence of outliers.

The left and right LFPs were high-pass filtered at 0.1 Hz and low-pass filtered at 50 Hz before decimation by a factor of 100 (from 10 kHz to 100 Hz). Outliers above four standard deviations were winsorized. The difference between left and right signals was calculated and a temporal variance filter with a 1 s rolling window was applied to the difference. A second four standard deviation filter was applied following this filtering. The subtraction step is intended to isolate the asymmetric stepping action of mice locomotion and the variance filter produces a strictly positive signal for comparison to animal velocity. The filtered electrographic signal and velocity were correlated. The square root of both signals was found to be more highly related than the signals (probably due to further reduction of outlier influence). Forward and backward phase shifts were applied at 10 ms resolution to find the range under which the correlation was stable (that is, the time shift for which the correlation was significantly reduced, $P < 0.05$).

A trial average motion onset analysis was performed defining onset as a change from below to above 10% of the maximum locomotion speed. For this analysis, velocity estimates were low-pass filtered at 25 Hz instead of 5 Hz (again zero-phase delay) for higher temporal precision at the expense of reduced accuracy in velocity. Initial brain activity relative to locomotion onset was detected using a temporally weight skew filter applied to our trial averaged activity measure. The minimum value of the filter closely corresponded to our visual assessment of activity onset for a 1 s filter integration window. For eight samples both the median and quartiles were not unique and as such the mid-range of closest values was used to determine these quantities.

Stereotactic viral injections. For all experiments utilizing CNS injections, 8- to 10-week-old mice were anesthetized using isoflurane and positioned in a stereotactic apparatus (model 940 small animal stereotaxic instrument with digital display, David Kopf Instruments). One microlitre pulled glass micropipettes were connected to a microinjection dispense system (Picospritzer III, Parker) and then attached to the stereotaxic apparatus. A total volume of 0.5–0.7 μl of virus was injected at any individual site at a flow rate of 100 nl min⁻¹. The micropipette was kept in place for 10 min and slowly withdrawn to prevent backflow. The dissected skin and muscle layers were sutured and buprenorphine (0.01 mg kg⁻¹) was administered post-surgery for analgesia. For confirmation of injection efficiency, mice were perfused and processed for immunohistochemistry, as described below, at the conclusion of experiments.

In vivo extracellular field potential recordings. An artificial cerebrospinal fluid (aCSF)-filled microelectrode with 30–50 μm tip was placed in the lumbar spinal cord (L1; 300 μm lateral to dorsal artery; 800 μm in depth) to record extracellular field potentials. Signals were recorded in DC mode with an Axoprobe 1A amplifier (Molecular Devices) and processed using pCLAMP8 software and Digidata 1320A (Molecular Devices) with a 125 kHz sampling rate. The signal was low-pass filtered from 2 kHz and averaged using Clampfit 10 from a minimum of nine traces, with all recorded traces being used in the analysis, offline. For the electrical stimulation of SI, twisted bipolar stimulation electrodes were made with polyimide-insulated stainless steel wires (outside diameter 0.125 mm; Plastics One) and placed in the SI (bregma -0.9 mm, lateral 1.9 mm and depth 0.5 mm) using stereotaxic instruments. Stimulation was applied via the PSIU6 stimulus isolation unit of a Grass S88 stimulator (Grass Technologies) with current between 0.1 and 0.2 mA and a duration of 0.2 ms. The stimulation interval was set at 5 s. For photostimulation of SI neurons, we recorded L1 field potentials from *Emx1::cre* (B6.129S2-*Emx1*^{tm1(cre)Kri}/J, Jackson Stock 005628) injected with AAV-*efla*-DIO-*hChR2-eYFP* into the SI area of *Emx1::cre* mice. A 200 μm optical fiber was used to stimulate the pyramidal neurons of the SI (bregma anteroposterior (AP) -0.9 mm, lateral 1.9 mm, dorsoventral (DV) 0.5 mm) for laser pulse stimulation. An 80 mW, 450 nm blue laser diode (Doric Lenses) modulated by an internal TTL pulse generator was used to photostimulate the SI region with single 5–10 ms light pulses with a power range of 1–10 mW as measured by a power meter (Thorlabs).

Retrograde labelling of lumbar projecting cells. CAV2-*cre* (0.4 μl; 2.5 × 10¹² vp ml⁻¹, Montpellier Vector Platform) was injected unilaterally into the ventromedial area of the L1 spinal level of Ai9 mice using the following coordinates: 300 μm lateral to dorsal artery; 800 μm depth. Mice were euthanized two weeks after injections. Mouse brains were fixed in 4% paraformaldehyde and were subsequently cryosectioned into 30 μm coronal sections. TdTomato visualization of retrograde CAV2-*Cre*-induced recombination was examined in SI and in two positive control regions: the locus coeruleus and the reticular formation.

In vitro recording of locomotor related activity and optogenetics. Neonatal (P0–3) pups from a cross of *Emx1::cre* (B6.129S2-*Emx1*^{tm1(cre)Kri}/J, Jackson Stock 005628) and Ai27D (B6.Cg-Gt(Rosa)26Sor^{tm27.1(CAG-COP4^{H134R}/tdTomato)Hze}/J, Jackson Stock 012567) mice underwent fictive locomotor recordings while the somatosensory cortex was stimulated optogenetically to determine its role in locomotion. The pups were anesthetized by cooling them in an ice bath. Whole spinal cord with hemibrain dissection was performed. Briefly, an anesthetized neonatal mouse was eviscerated in cold oxygenated (95% O₂ and 5% CO₂) low-calcium aCSF composed of 111 mM NaCl, 3.1 mM KCl, 25 mM NaHCO₃, 1.1 mM KH₂PO₄, 7.6 mM MgSO₄, 0.33 mM CaCl₂ and 11 mM glucose. Under a dissection microscope (LEICA MS-5), the skull and dorsal half vertebrae were removed with fine scissors and forceps. Half of the brain, the brainstem and the spinal cord were then dissected out carefully using the fine scissors. The preparation was then transferred to a recording chamber with three compartments. The thoracic and lumbar segments were placed ventral side up. The hemibrain was then positioned dorsal side up. The cervical spinal cord segment was aligned in the middle compartment. Latex membranes and a mixture of high-vacuum grease and Vaseline to prevent solution leakage between compartments separated these three compartments. All three compartments were superfused with oxygenated (95% O₂ and 5% CO₂) aCSF composed of 111 mM NaCl, 3.1 mM KCl, 25 mM NaHCO₃, 1.1 mM KH₂PO₄, 1.25 mM MgSO₄, 3.3 mM CaCl₂ and 11 mM glucose at room temperature (22 ± 0.5 °C). KA (2 mM) was administered to the compartment containing the brain and brainstem to block the glutamatergic synaptic transmission and cortical processing. NMDA (5–7 μM) and 8–10 μM 5-HT were added to the lumbar segment compartment to evoke locomotor-related activity. For experiments examining the necessity of cervical excitatory connectivity for the SI control of locomotion, 2 mM KA was administered to the compartment containing the cervical segment to block the glutamatergic synaptic transmission within the cervical spinal cord. A 200 μm optical fiber was placed on the surface of the sensory cortex for laser pulse stimulation. An 80 mW, 450 nm blue laser diode (Doric Lenses) controlled by an internal TTL pulse generator was used to stimulate the SI region (3.0 mm caudal from the olfactory bulb and 1.2 mm lateral from the midline). Pulse trains consisting of 15 pulses of 10 ms at 30 Hz were

performed at 2 s intervals with a power range of 1–10 mW as measured by a power meter (Thorlabs). Tight-fitting bipolar suction electrodes (A-M Systems) filled with a bath of aCSF were used to record neurograms from the right or left L2 and L5 ventral roots. Neurograms were amplified (1,000 times) using an Axoprobe 1A device and a preamplifier, 1 kHz low-pass and 100 Hz high-pass filtered, digitized (Digidata 1320A; Molecular Devices), acquired with Clampex 8 software (Molecular Devices), and saved on a laboratory computer for offline analysis.

Anterograde tracing of cervical-projecting SI pyramidal neurons. AAVDJ-*Syn1-DIO-eGFP* (Salk Vector Core – 2.31×10^{12} genome copies (GC)/mL) was injected unilaterally into the SI area of *Emx1::cre* mice as described above. Serial transverse sections from C1 to T2 spinal levels were imaged using an Aperio ScanScope AT2 whole slide scanner to examine for eGFP-positive projection patterns from SI pyramidal neurons to the cervical spinal cord.

Pharmacogenetic stimulation and inhibition of somatosensory locomotor neurons. To target the somatosensory locomotor neurons we initially bilaterally injected CAV2-*cre* into the C4–5 spinal level of C57BL/6J mice, as described above. Two weeks later, AAVs carrying double-floxed *hM3Dq* excitatory DREADD (AAV5-*DIO-hM3Dq-mCherry*, 3.8×10^{12} GC mL⁻¹, UNC Vector Core) and FLEX^{loxP} inhibitory PSAM (AAVDJ-*syn::FLEX^{loxP}-rev::PSAM^{L141F}-GlyR-IRES-GFP*, 1.0×10^{12} GC mL⁻¹; plasmid was a gift from S. Sternson, Addgene plasmid no. 32479) were injected bilaterally into layer V of the SI following the coordinates described above. Mice were allowed two to four weeks of rest following injections to allow full expression of constructs. For SI activation experiments, CNO in saline was administered intraperitoneally (2 mg kg⁻¹) and behavioral effects were measured 2.5 h later. For SI silencing, PSEM₃₀₈ in saline was administered intraperitoneally (5 mg kg⁻¹) and behavioral effects were measured 10 min later.

Retrograde labeling of *Vglut2*⁺ lumbar-projecting cervical neurons. CAV2-*FLEX^{loxP}-Flp* was unilaterally injected into the L1 spinal level of *Vglut2::cre*;Ai65 hybrid mice at the following coordinates: 300 μm lateral to dorsal artery; 800 μm depth. Mice were euthanized two weeks later and spinal cords were subsequently fixed in 4% PFA and cryosectioned from thoracic level T1 to cervical level C2. tdTomato-DAPI-positive cells were counted in each spinal lamina. The coordinates of the tdTomato-DAPI positive cells were used in a custom MATLAB script used for the three-dimensional reconstructions.

Behavioral analyses. For measurement of spontaneous locomotor activity in an open field, individual mice were placed in a 55 × 27.5 cm polypropylene box and recorded using an overhead camera following a 15 min period of acclimatization. Following this, mice were injected with either saline or PSEM³⁰⁸ intraperitoneally. Activity was recorded for the 30 min following injection and analyzed using SMART video tracking software (Panlab). For Catwalk (Noldus) gait analysis, mice performed walks before and 10 min after PSEM³⁰⁸ injection. SI stimulation experiments using CNO were performed in an analogous manner except that injections were performed 2.25 h before open field acclimatization. Catwalk and locomotor kinematics runs were performed 2.5 h after CNO administration. Kinematics videos were collected with a Promon 501 high-speed camera (AOS Technologies) at 90 f.p.s. and analyzed with MaxTRAQ software (Innovision Systems).

To examine any pain-related effects induced by pharmacogenetic stimulation of SI neurons, mice underwent a von Frey test. Each mouse was placed in a wire mesh cage and habituated for 30 min before testing. Calibrated von Frey filaments (0.008–300 g, The Touch Test von Frey filaments, North Coast Medical) were pressed into each paw until it was bent. Three withdrawals out of the five touches were considered to be the positive threshold stimulus. Filaments were applied in ascending order and the lowest weight of filament that produced a positive response was considered the threshold stimulus. Response to thermal noxious stimuli was assessed using the tail flick test, in which the latency of tail withdrawal in response to a thermal stimulus was measured. Each animal was individually restrained and the tail was held under the Tail Flick Analgesia Meter, a specially designed apparatus combining a heat lamp and movement sensor (IITC Life Sciences). Withdrawal of the tail resulting from the lamp's heat was automatically detected by the sensor and the withdrawal latency was recorded in three trials.

The forelimb grip strength of mice before and after silencing of the sensory pathway was assessed using the SDI Grip Strength System model DFM-10; (San Diego Instruments). Each mouse was tested for five consecutive trials and the average grip force was calculated.

Silencing of SI-lumbar field potentials through inhibition of glutamatergic cervical neurons. In vivo electrophysiology experiments were prepared as previously described with electrical stimulation of the SI during concurrent recording in the ventromedial portions of lumbar (L1) regions. Conditional expression of inhibitory chimeric ion channel PSAM-GlyR^{L141F;Y115F} in lumbar-projecting cervical glutamatergic neurons was achieved through sequential bilateral injections of CAV2-*FLEX^{loxP}-Flp* (2.5×10^{12} vp mL⁻¹, Montpellier Vector Platform) into the ventromedial area of the L1 spinal level of *Vglut2::cre* mice using the following coordinates: 300 μm lateral to the dorsal artery; 800 μm depth.

Two weeks later, bilateral AAV9-*FLEX^{FRT}-PSAM^{L141F;Y115F}-GlyR* (plasmid was a gift from S. Arber, AAV generated by UNC Vector Core – 1.9×10^{13} GC ml) was injected into the C4–C5 spinal level using the following coordinates: 500 μm lateral to the dorsal artery; 600 μm depth. Mice were allowed two to four weeks of rest following the last injections to allow full expression of constructs before electrophysiology experiments. PSEM₃₀₈ (5 mg kg⁻¹, Apex Scientific) in saline was administered intraperitoneally via a catheter to transiently silence the PSAM expressing lumbar projecting cervical glutamatergic neurons.

Cellular specific monosynaptic tracing. The cTRIO (cell-type specific system for tracing input and output) methodology was performed as previously described. Briefly, CAV2-*FLEX^{loxP}-Flp* (2.5×10^{12} GC mL⁻¹) was injected unilaterally into the ventromedial area of L1 (300 μm lateral to the dorsal artery, 800 μm depth) to selectively express flippase in glutamatergic neurons projecting to the rhythmic region of the lumbar locomotor CPG in *Vglut2::cre* mice. Two weeks later, a mix (1:1 in a total volume of 0.5 μl) of AAV9-*FLEX^{FRT}-TC* and AAV9-*FLEX^{FRT}-G* (plasmids were gifts from L. Luo, AAVs generated by UNC Vector Core – 2.2×10^{13} and 1.8×10^{13} GC mL⁻¹, respectively) was injected ipsilaterally into the cervical spinal cord (C4–C5: 300 μm lateral to the dorsal artery, 800 μm depth) to express TVA receptor and rabies glycoprotein in lumbar-projecting glutamatergic neurons selectively expressing flippase. Two weeks after these injections, EnvA-pseudotyped rabies virus lacking rabies glycoprotein (EnvA-RB-DG 1.30 × 10⁹, provided by GT3 Viral Vector at the Salk Institute) was injected in the same region of the cervical spinal cord. Mice were euthanized two weeks later and brain, brainstem and spinal cord were subsequently fixed in 4% PFA and cryosectioned. Brains were coronal sectioned at 80 μm. Reconstruction of the brains with simultaneous visualization of sensory cortex neurons dysynaptically connected to lumbar spinal cord was performed using StereoInvestigator (MBF, Bioscience).

Anterograde tracing of lumbar-projecting cervical neurons. *Vglut2::cre* animals were bred into the Ai9 (*Rosa26^{FLEx-tdTomato}*) Cre reporter strain. AAVDJ-*Syn1-DIO-eGFP* (Salk Vector Core – 2.31×10^{12} GC mL⁻¹) was injected unilaterally into the C4–C5 spinal level as described above. eGFP-positive projections from cervical glutamatergic neurons were visualized in serial transverse sections from T13 to S1. eGFP projections were counted in each designated lamina (Paxinos) for all relevant spinal cord segments using NeuroLucida 360 software (MBF Bioscience).

Immunohistochemistry. Brains and cervical and lumbar spinal cords were removed and fixed for 2 h in 4% PFA in PBS, rinsed in PBS, cryoprotected in 30% (wt/vol) sucrose in PBS overnight and embedded in OCT mounting medium. Coronal sections (30 μm) of the brains and spinal cords were obtained on a cryostat for immunohistochemistry. Sections were incubated overnight at 4 °C with the primary antibody anti-choline acetyltransferase antibody (mouse, 1:100, Millipore, MAB305). Alexa Fluor 568-conjugated secondary antibody was incubated for 1 h at room temperature to visualize immunoreactive sites. Slides were rinsed, mounted in Vectashield mounting medium (Vectorlabs) and scanned on LSM510 and LSM880 confocal microscopes (Zeiss Microsystems). Multiple channels were scanned sequentially to limit fluorescence bleedthrough and false-positive signals. Images of whole-brain sections stained with H&E were taken using the Aperio ScanScope AT2 whole slide scanner.

Statistics and analysis. Sample size was selected based on previous experiments from our lab and others using the neurobehavioral and electrophysiological techniques described. Because only within-subject experimental designs were used, no randomization method was used and the investigators were not blinded during the experimental procedures. However, to control for possible carryover effects, the order of saline, PSEM and CNO treatments were varied across behavioral experiments. All animals that met the experimental conditions were analyzed. In accordance with *Nature Neuroscience's* data reporting and reproducibility standards, additional information regarding data collection practices can be found in the accompanying Life Sciences Reporting Summary. All statistical tests were performed using SPSS v21 (IBM), and graphs were generated using PRISM 6 (GraphPad Software). Graphs represent the mean ± s.e.m. unless noted otherwise. Assumptions of parametric statistical tests, such as normal data distribution and homoscedasticity were met in cases where paired *t*-test and repeated-measures ANOVA were used. In experiments where data did not meet the assumption of normality, non-parametric tests such as the Wilcoxon signed-rank test or the two-sample Kolmogorov–Smirnov test were used to compare paired samples or data distributions, respectively. Correlation between variables was examined via Pearson correlation (Fig. 1d). Distributions of data were compared using repeated-measures ANOVA with Tukey's post-hoc test (Fig. 4c), repeated measures ANOVA with Dunnett's multiple comparisons post-hoc test (Fig. 5c,e and Extended Data Fig. 5a–e), two-sample Kolmogorov–Smirnov test (Figs. 2d,e and 6a), Wilcoxon matched-pair sign-rank test (Fig. 6b), paired Student's *t*-test (Fig. 7c and Extended Data Figs. 2b, 6, 7a,b and 8) and Friedman test (Extended Data Fig. 3c,d). Two-tailed statistical tests were used exclusively for all applicable analyses. All test statistics, *P* values, sample sizes, degrees of freedom and effect size estimates for these statistical analyses are provided in Supplementary Tables 1 and 2. Effect size estimates were calculated using G*Power. For lumbar LFP data (Fig. 2), spike

probability distributions were generated by binning data in 1 ms increments and binarizing based on the average measurement for the recorded trial. Shuffle distributions of the LFP data were generated by shuffling trial data 1,000 times and averaging the resultant shuffled data. Shuffle operations were performed with Python 3.6 using the pyABF, NumPy and Pandas libraries. Phase dispersion polar plots were plotted in R (R Foundation for Statistical Computing, 2005, <http://www.r-project.org>).

Reporting Summary. Further information on research design is available in the Nature Research Reporting Summary linked to this article.

Data availability

Source data have been provided for Figs. 1c,d (values in Fig. 1d are the square root of values in Fig. 1c), 2d,e, 4c, 5c,e, 6a,b and 7c. Source data have also been provided for Extended Data Figs. 2b, 5a–c,e, 6, 7a,b and 8. Any additional data pertaining to this manuscript is available from the authors upon reasonable request.

Code availability

Any custom script or code used in this study is available from the authors upon reasonable request.

Acknowledgements

This research was supported by CIHR Grant MOP13683 (M.G.F.), CIHR Grant MOP 86470 (S.G.), an AOSPINE Young Investigator Research Grant (K.S.), the Halbert Chair in Neural Repair and Regeneration (M.G.F.) and the DeZwirek Foundation (M.G.F.). S.K.K. was supported by the Onassis Foundation. We thank C. Castro and

S. Sivakumaran for technical assistance and S. Arber for the FLEX^{FRT}-PSAM^{L141EY115F}-GlyR plasmid (Friedrich Miescher Institute).

Author contributions

S.K.K., K.S. and M.G.F. designed all experiments. S.K.K. performed viral tracings, anatomical investigations, behavioral experiments and data analysis. K.S. performed viral tracings, anatomical investigations, behavioral experiments, all electrophysiological recordings and data analysis. A.M.L. performed the molecular and viral work, behavioral experiments, data analysis and statistics. L.L. provided technical assistance with the in vitro and in vivo lumbar field potential recordings. D.R. performed behavioral tracking and electrophysiology data analysis for the in vivo SI-cortical recording in freely moving mice. I.W. participated in the cortical electrode implantations. S.K.K., K.S., S.G., A.M.L. and M.G.F. wrote the paper, with contributions from D.R. M.G.F. supervised the work and provided the funding for the work.

Competing interests

The authors declare no competing interests.

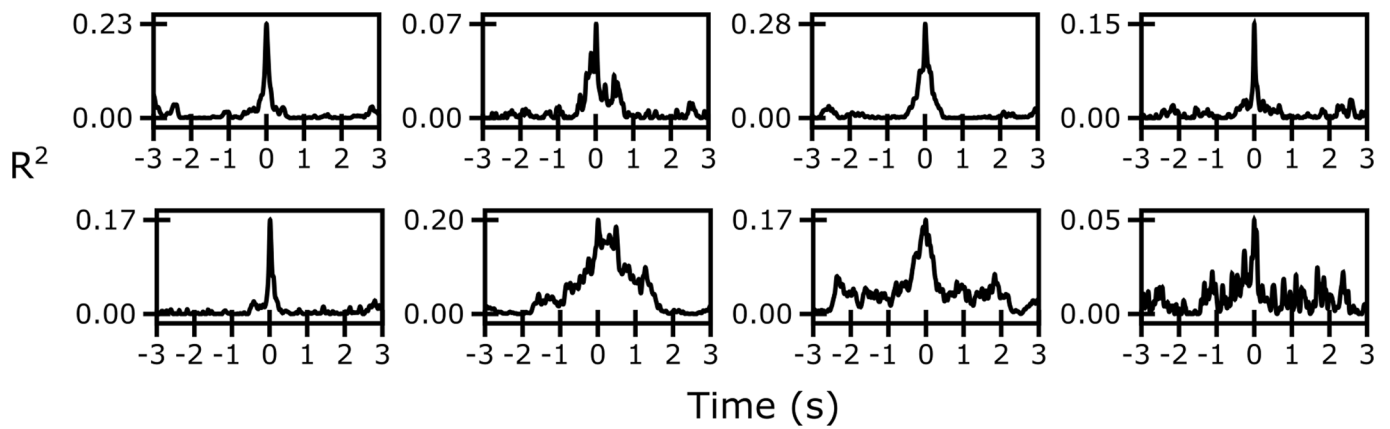
Additional information

Extended data is available for this paper at <https://doi.org/10.1038/s41593-019-0536-7>.

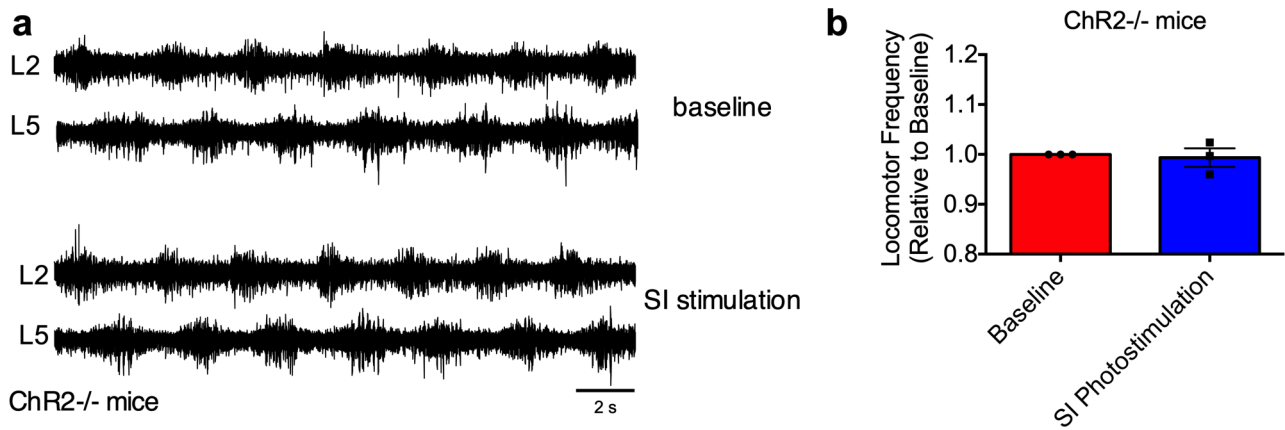
Supplementary information is available for this paper at <https://doi.org/10.1038/s41593-019-0536-7>.

Correspondence and requests for materials should be addressed to S.K.K., K.S. or M.G.F.

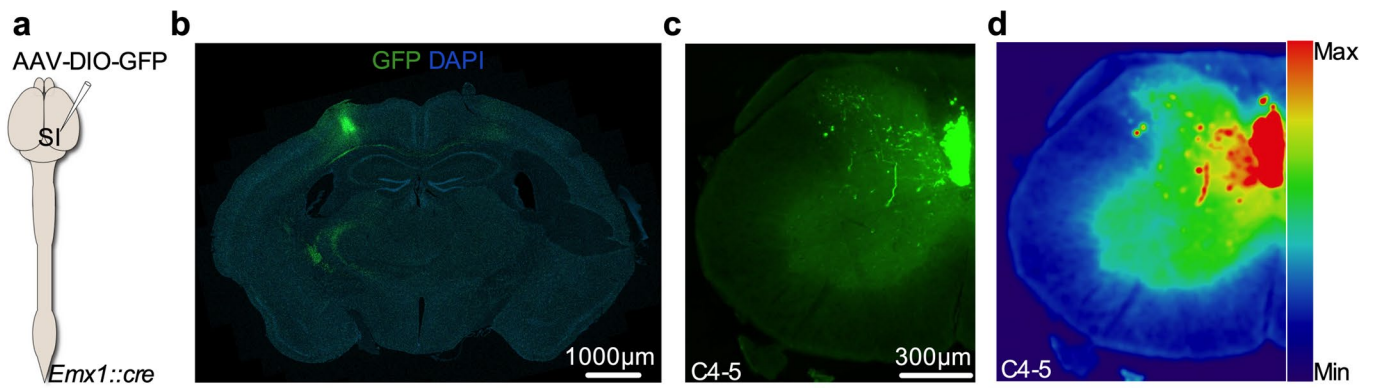
Reprints and permissions information is available at www.nature.com/reprints.



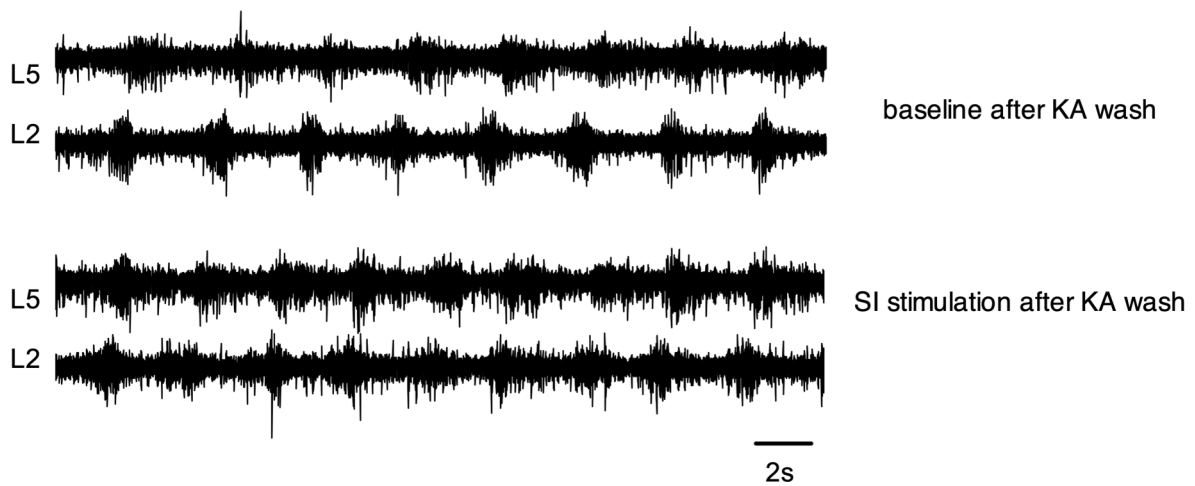
Extended Data Fig. 1 | Decorrelation analysis of animal velocity and somatosensory activity. Decorrelation of animal velocity and somatosensory activity from panel Fig. 1(c) across artificially shifted temporal correspondence. The correlation plots in Fig. 1(d) correspond to relationship at the zero temporal shift. Positive shift time corresponds to velocity compared to latter somatosensory activity. (n=8 mice).



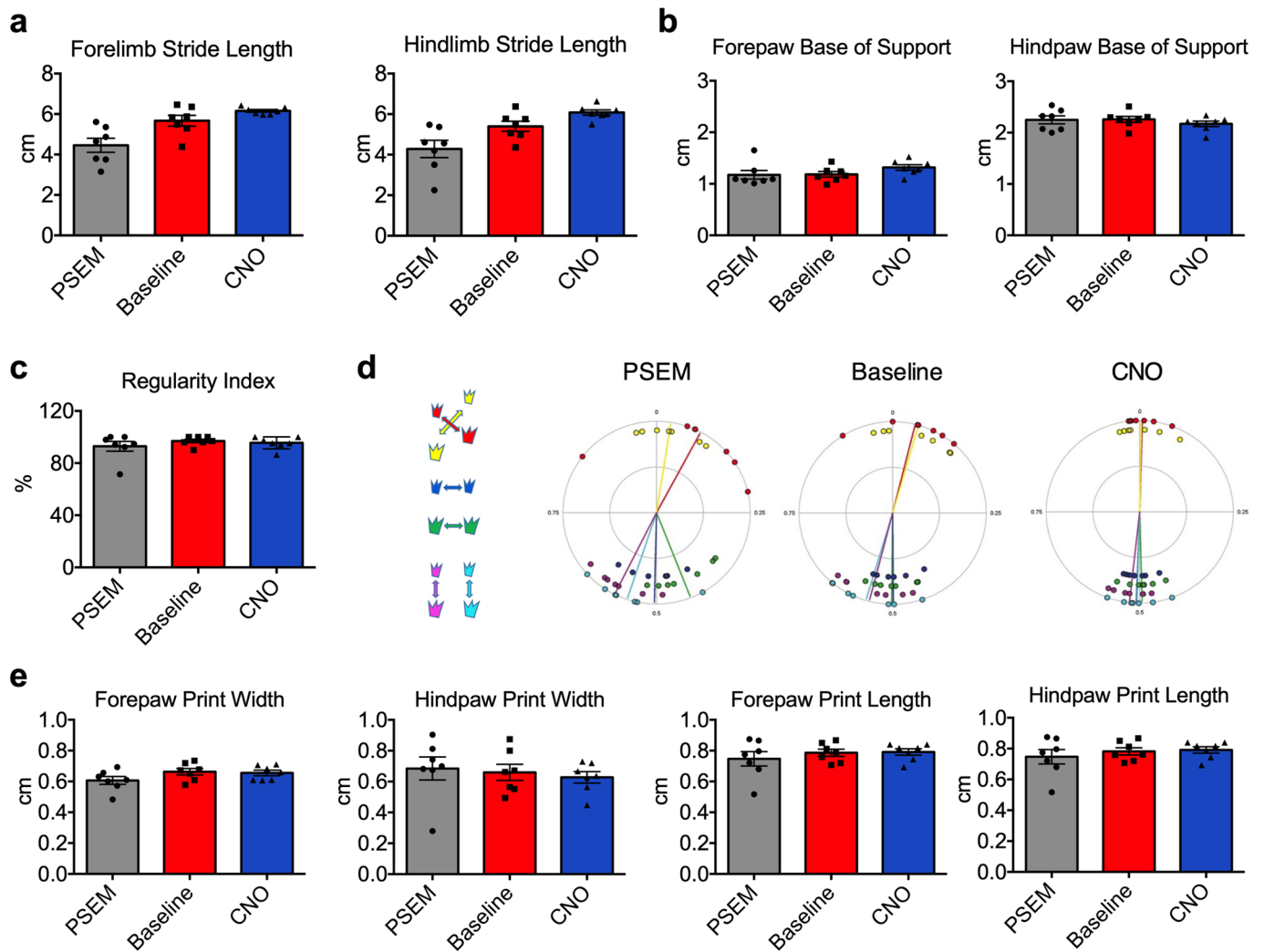
Extended Data Fig. 2 | Control SI stimulation in ChR2^{-/-} mice does not increase locomotor frequency. **a**, Representative ENG recordings of locomotor like activity from ipsilateral L2 and L5 ventral roots induced with 7 μ M NMDA and 10 μ M 5-HT. of a ChR2^{-/-} mice (baseline). Optogenetic stimulation of the SI neurons in these mice did not evoke an increase in the frequency of locomotor-related burst activity (SI stimulation) (bottom). **b**, Relative change in frequency of locomotor-like activity before optical stimulation of SI (red) and during SI optical stimulation (blue) in ChR2^{-/-} mice. No significant difference was revealed between the two conditions (two-tailed paired t-test, $p=0.759$). $n=3$ mice. Group data are presented as mean \pm s.e.m.



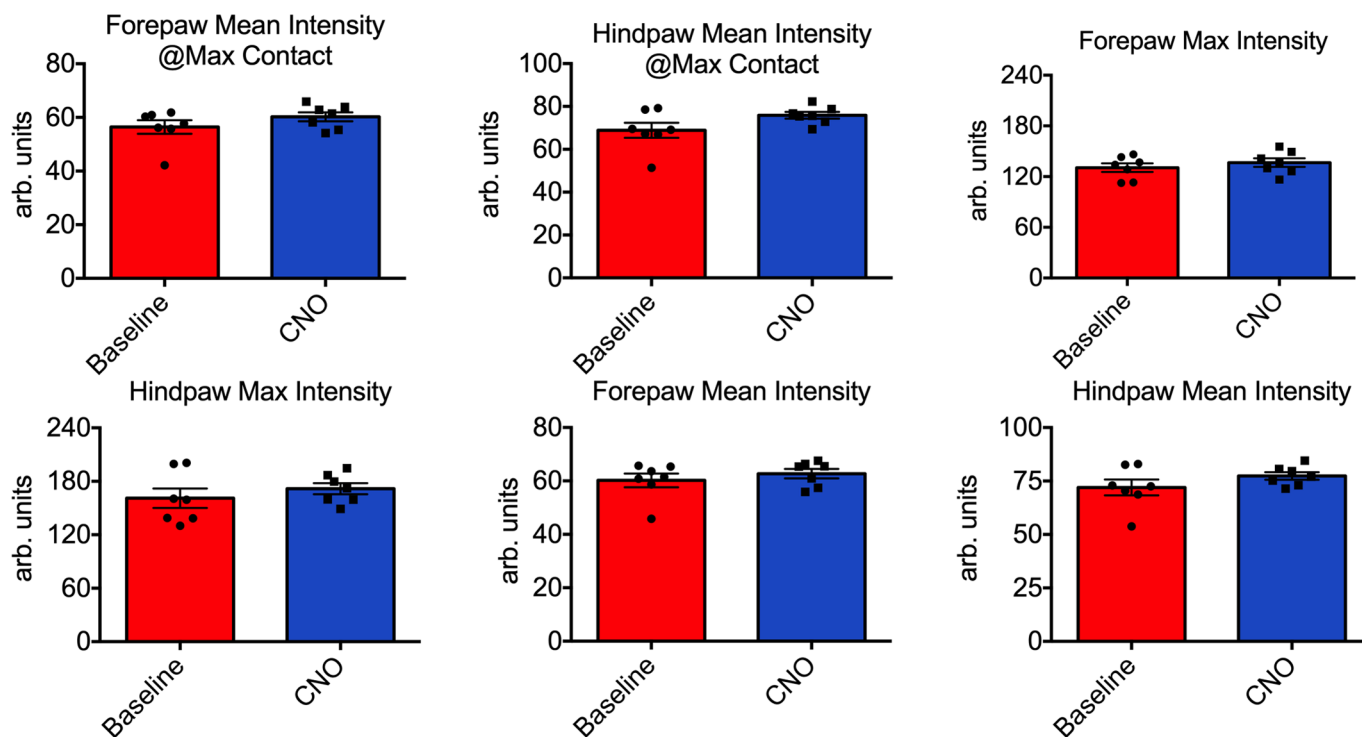
Extended Data Fig. 3 | SI pyramidal neurons project to intermediate gray zone of cervical spinal cord. **a**, AAVDJ-*syn1*-DIO-EGFP were injected unilaterally into *Emx1::cre* mice ($n = 3$). **b**, SI pyramidal neurons expressing GFP at the AAVDJ-*syn1*-DIO-EGFP injection site. **c**, Confocal images of 30 µm-thick transverse sections of the cervical spinal cord of the same animal contained eGFP⁺ projections in the intermediate gray matter of C4-7. **d**, Heat map reveal dense projections mainly in the intermediate gray zone.



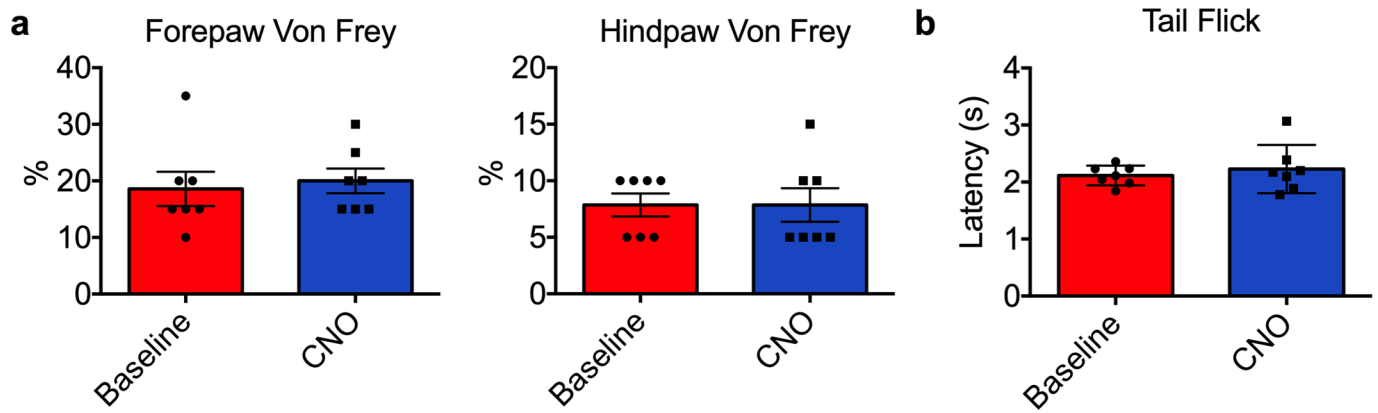
Extended Data Fig. 4 | Effect of SI stimulation on locomotion after KA washout. Baseline ENG recordings of locomotor like activity from ipsilateral L2 and L5 ventral roots of a P0-3 *Emx1::cre; Ai27D* offspring one hour after KA perfusion in the cervical cord has been terminated (Top). Optogenetic stimulation of the SI neurons one hour after KA perfusion in the cervical cord has been terminated increases the frequency of locomotor-like bursting activity. ($n = 4$ mice) (Bottom).



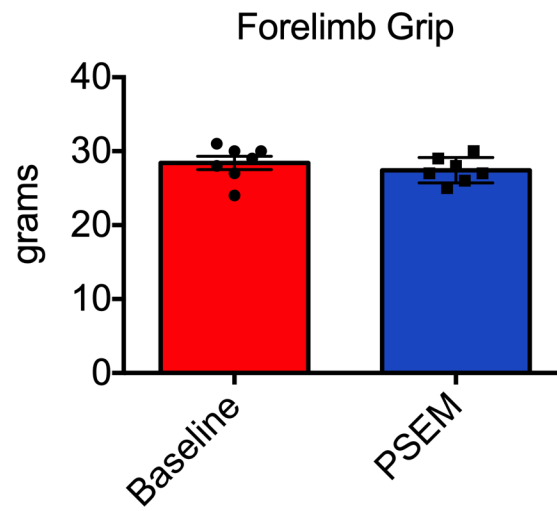
Extended Data Fig. 5 | Manipulation of the SI locomotor pathway does not change the general locomotor capability. **a**, Bar graphs showing no change in the stride length after CNO administration. **b**, Bar graphs demonstrating the forepaw and hindpaw base of support before and after PSEM or CNO administration. **c**, Regularity index of mice before and after manipulation of the SI locomotor pathway. **d**, Circular diagrams showing that phase dispersions consistent with the trot gait pattern were preserved after silencing or activation of the SI locomotor pathway. **e**, Bar graphs demonstrate the lack of effects of the manipulation of the sensory locomotor pathway on the print width and print length of both forepaws and hindpaws. Data were extracted using Catwalk XT software (repeated measures one-way ANOVA with Dunnett's multiple comparisons test, * indicates $p < 0.05$, $n = 7$ mice). Group data are presented as mean \pm s.e.m.



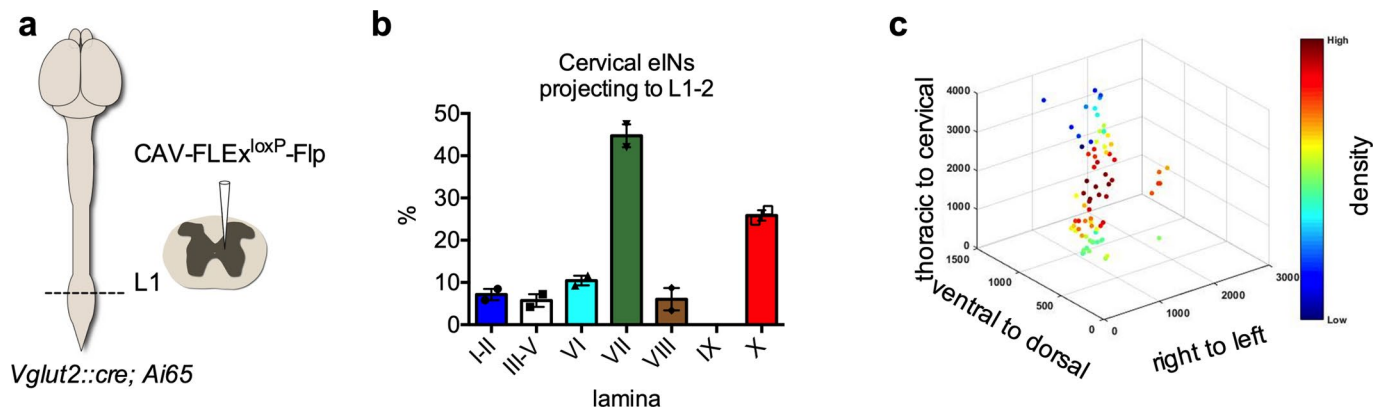
Extended Data Fig. 6 | Stimulation of the SI locomotor pathway does not induce neuropathic pain. Bar graphs showing the intensity of signal obtained from forepaws and hindpaws during locomotion on the Catwalk gait analysis system do not change after CNO administration. Data were analyzed using two-tailed paired t-tests ($n=7$ mice). No statistically significant differences were observed (Related to Fig. 3). Group data are presented as mean \pm s.e.m.



Extended Data Fig. 7 | Stimulation of the SI locomotor pathway does not change the reaction to noxious stimuli. a, Bar graphs showing the frequency of forepaw and hindpaw withdrawal resulting from 10 non-consecutive touches on each paw with the 0.4 g von Frey monofilament during both baseline and CNO conditions. **b**, Bar graph showing the latency to withdrawal of the tail following exposure to mild thermal stimulus in both baseline and CNO conditions, with each data point representing the average of three trials. Data were analyzed by two-tailed paired t-test ($n = 7$ mice). No statistically significant differences were observed. Group data are presented as mean \pm s.e.m.



Extended Data Fig. 8 | Inactivation of the SI neurons projecting to cervical cord does not decrease the forelimb strength. Bar graph showing mean grip strength for mice before and after PSEM injection to inhibit SI neurons. Data were analyzed by two-tailed paired t-test ($n=7$ mice). No statistically significant differences were observed. Group data are presented as mean \pm s.e.m.



Extended Data Fig. 9 | Anatomical distribution of the cervical excitatory cells projecting to ventromedial region of upper lumbar spinal cord. a, *Vglut2::cre* mice were crossed with an Ai65(RCFL-tdT) line that contains FRT-stop-FRT and LoxP-stop-LoxP double cassettes ahead of *tdTomato*. Laminae VII/VIII/X of L1 spinal segments of adult *Vglut2::cre*;Ai65(RCFL-tdT) were unilaterally injected with the retrograde virus CAV2-FLEX^{loxP}-Flp ($n=2$ mice). **b**, Laminar distribution of the tdTomato-positive lumbar-projecting cervical glutamatergic cells. **c**, Density plot demonstrating the distribution of the lumbar projecting glutamatergic cells in the cervical enlargement. Group data are presented as mean \pm s.e.m.

Reporting Summary

Nature Research wishes to improve the reproducibility of the work that we publish. This form provides structure for consistency and transparency in reporting. For further information on Nature Research policies, see [Authors & Referees](#) and the [Editorial Policy Checklist](#).

Statistics

For all statistical analyses, confirm that the following items are present in the figure legend, table legend, main text, or Methods section.

- | | |
|-----|-----------|
| n/a | Confirmed |
|-----|-----------|
- The exact sample size (n) for each experimental group/condition, given as a discrete number and unit of measurement
 - A statement on whether measurements were taken from distinct samples or whether the same sample was measured repeatedly
 - The statistical test(s) used AND whether they are one- or two-sided
Only common tests should be described solely by name; describe more complex techniques in the Methods section.
 - A description of all covariates tested
 - A description of any assumptions or corrections, such as tests of normality and adjustment for multiple comparisons
 - A full description of the statistical parameters including central tendency (e.g. means) or other basic estimates (e.g. regression coefficient) AND variation (e.g. standard deviation) or associated estimates of uncertainty (e.g. confidence intervals)
 - For null hypothesis testing, the test statistic (e.g. F , t , r) with confidence intervals, effect sizes, degrees of freedom and P value noted
Give P values as exact values whenever suitable.
 - For Bayesian analysis, information on the choice of priors and Markov chain Monte Carlo settings
 - For hierarchical and complex designs, identification of the appropriate level for tests and full reporting of outcomes
 - Estimates of effect sizes (e.g. Cohen's d , Pearson's r), indicating how they were calculated

Our web collection on [statistics for biologists](#) contains articles on many of the points above.

Software and code

Policy information about [availability of computer code](#)

Data collection

Gait Video Acquisition: Catwalk 10.6 XT (Noldus). Kinematics Video Acquisition: AOS Promon Studio (501). Open Field Acquisition: Panlab SMART v2.0. SI Activity/Movement Recordings: Micro-manager version 1.4.19 with MMCore version 6.2.0 and paired ImageJ 1.48v with Java 1.6.0_31. Camera driver was QCamDriver DLL version 2.0.12 provided by QCapture 2.9.12. Electrophysiological recordings: Spike2 8.14 x64 (1401 driver, CED Systems), pClamp v8 (Molecular Devices), Clampex 8 (Molecular Devices).

Data analysis

Gait Analysis: Catwalk 10.6 XT (Noldus). Kinematic analysis: MaxTRAQ 2d. Open Field Analysis: Panlab SMART v2.0. Electrophysiology Analysis: Spike2 8.14 x64 (1401 driver, CED Systems), pClamp v8 (Molecular Devices), Clampfit 10 (Molecular Devices). Shuffle operations: Python 3.6 using the pyABF, NumPy, and Pandas libraries. Image/Cellular Analyses: NeuroLucida 360 (MBF Bioscience), StereoInvestigator (MBF Bioscience). Phase dispersion polar plots: R (v3.1.2). Heatmap plots: Matlab (v9.1) custom script. Effect Size Estimates: G*Power. Graphs/Statistics: Graphpad Prism 6.00. Statistics: IBM SPSS v21.0.0.0.

For manuscripts utilizing custom algorithms or software that are central to the research but not yet described in published literature, software must be made available to editors/reviewers. We strongly encourage code deposition in a community repository (e.g. GitHub). See the Nature Research [guidelines for submitting code & software](#) for further information.

Data

Policy information about [availability of data](#)

All manuscripts must include a [data availability statement](#). This statement should provide the following information, where applicable:

- Accession codes, unique identifiers, or web links for publicly available datasets
- A list of figures that have associated raw data
- A description of any restrictions on data availability

Source data has been provided for Figures 1c/d (1d is the square-root of 1c values), 2d & e, 4c, 5c & e, 6a & b, and 7c. Source data has also been provided for Extended data figures 2b, 5a-c & e, 6, 7a & b, and 8. Any additional data pertaining to this manuscript is available upon reasonable request.

Field-specific reporting

Please select the one below that is the best fit for your research. If you are not sure, read the appropriate sections before making your selection.

Life sciences Behavioural & social sciences Ecological, evolutionary & environmental sciences

For a reference copy of the document with all sections, see [nature.com/documents/nr-reporting-summary-flat.pdf](https://www.nature.com/documents/nr-reporting-summary-flat.pdf)

Life sciences study design

All studies must disclose on these points even when the disclosure is negative.

Sample size	Sample size was selected based on previous experiments from our lab and others using the neurobehavioural and electrophysiological techniques described.
Data exclusions	All results that met experimental criteria (ie. correct placement of electrodes) were analyzed. No data were excluded.
Replication	Multiple lines of evidence were used (ie. optogenetic and chemogenetic experiments, behavioural and electrophysiological outcomes, etc) to support the main conclusions of the manuscript, providing additional confidence in the robustness of the findings. All replication attempts using these varied methodologies were successful.
Randomization	Since only within-subject experimental designs were used, no randomization method was used for the experimental procedures. However, to control for possible carryover effects, the order of saline, PSEM, and CNO treatments were varied across behavioural experiments.
Blinding	Since only within-subject experimental designs were used, no randomization method was used for the experimental procedures. However, to control for possible carryover effects, the order of saline, PSEM, and CNO treatments were varied across behavioural experiments.

Reporting for specific materials, systems and methods

We require information from authors about some types of materials, experimental systems and methods used in many studies. Here, indicate whether each material, system or method listed is relevant to your study. If you are not sure if a list item applies to your research, read the appropriate section before selecting a response.

Materials & experimental systems

n/a	Involved in the study
<input checked="" type="checkbox"/>	<input type="checkbox"/> Antibodies
<input checked="" type="checkbox"/>	<input type="checkbox"/> Eukaryotic cell lines
<input checked="" type="checkbox"/>	<input type="checkbox"/> Palaeontology
<input type="checkbox"/>	<input checked="" type="checkbox"/> Animals and other organisms
<input checked="" type="checkbox"/>	<input type="checkbox"/> Human research participants
<input checked="" type="checkbox"/>	<input type="checkbox"/> Clinical data

Methods

n/a	Involved in the study
<input checked="" type="checkbox"/>	<input type="checkbox"/> ChIP-seq
<input checked="" type="checkbox"/>	<input type="checkbox"/> Flow cytometry
<input checked="" type="checkbox"/>	<input type="checkbox"/> MRI-based neuroimaging

Animals and other organisms

Policy information about [studies involving animals](#); [ARRIVE guidelines](#) recommended for reporting animal research

Laboratory animals	This study used the following strains and transgenic mouse lines: C57BL/6J mice (Jackson Labs: #000664), Vglut2::cre mice (B6-Slc17a6tm2(cre)Lowl/J, Jackson Labs: # 016963), Ai9 mice (B6.129S-Gt(Rosa)Sor26tm9(CAG-tdTomato)Hze/J Jackson Labs: #007908), Ai65 mice (B6.129S-Gt(Rosa)Sor26tm65.1(CAG-tdTomato)Hze/J, Jackson Labs: #021875), Ai27D mice (B6.Cg-Gt(ROSA)26Sortm27.1(CAG- -COP4*H134R/tdTomato)Hze/J, Jackson Labs: #012567) and Emx1::cre mice (B6.129S2-Emx1tm1(cre)Krl/J, Jackson Labs: #005628). Experiments were performed on mice 8-12 weeks old.
Wild animals	Study did not involve wild animals.
Field-collected samples	Study did not involve samples collected from the field.
Ethics oversight	The University Health Network Animal Research Committee provided review and oversight of the work performed herein.

Note that full information on the approval of the study protocol must also be provided in the manuscript.